Friedrich-Schiller-Universität Jena
Physikalisch-Astronomische Fakultät

Adjoint Quarks in Technicolor and QCD

Master Thesis

Zur Erlangung des akademischen Grades
Master of Science Physik

Betreuer:	*Dr. Axel Maas*
1. Korrektor:	*Dr. Axel Maas*
2. Korrektor:	*Prof. Dr. Holger Gies*
eingereicht:	*Oktober 2012*
vorgelegt von:	*Daniel August, geb. am 04.01.1989 in Eisenach*

Acknowledgments

At this point I would like to take the opportunity to thank all the people who supported me during my studies and writing this thesis.
First I want to thank my supervisor Dr. Axel Maas who supported me throughout this thesis. On one hand he helped me with the programing part and on the other hand he took always the time to explain the physical background. Furthermore he also gave helpful comments for the script of this master thesis.
I want to thank also my whole family, especially my parents and my grandparents, who supported me throughout these five years.

Abstract

Strongly interacting theories with adjoint fermions play an important role in theoretical physics. Looking at QCD for zero baryonic mass we find that the phase transition temperature for deconfinement and chiral symmetry breaking coincide. If we change the representation to the adjoint these temperatures do not coincides. This change gives rise to a new interesting phase which we do not observe for QCD with fundamental quarks. For this reason it is interesting to take a closer look into this theory to learn more about confinement and chiral symmetry breaking. In this thesis we focus on quenched SU(2)
An other strongly interacting theory with adjoint fermions is minimal walking technicolor. This theory is an extension to the standard model which replaces the Higgs with a bound state composed of technigluons and techniquarks. This extension to the standard model solves the hierarchy problem. Furthermore the study of this theory gives us more insight into strongly interacting theories. In this work we study the quark propagator for both theories on the lattice. We find for quenched SU(2) that the quark mass function is in accordance with the perturbation theory. Calculating the Schwinger function for this propagator we find a zero crossing which tells us that a sing quark is an unphysical particle. Performing the same calculation for the minimal walking technicolor we derive the anomalous mass dimension from the mass function. We find that this quantity is small compared to one which is in accordance with previous indirect calculations of this value. Looking again at the Schwinger function we can extract the mass of the techniquarks.

Contents

1 Introduction **1**

2 Minimal Walking Technicolor **3**
2.1 Electroweak Symmetry Breaking . . . 3
2.2 Fermion masses . . . 3
2.3 Walking . . . 4
2.4 Minimal Walking Technicolor . . . 5
2.5 Quark Propagator . . . 6

3 QCD on the lattice **7**
3.1 Strongly interacting field theories . . . 7
3.2 Euclidean space . . . 8
3.3 Introducing the lattice . . . 9
3.4 Link variables . . . 10
3.5 Dirac Propagator . . . 12

4 Methods **15**
4.1 The quenched approximation . . . 15
4.2 Unphysical particles and the Schwinger function . . . 15
4.3 Antiperiodic boundaries . . . 17
4.4 Calculating the A and B function . . . 17
4.5 Lattice corrections . . . 19
4.6 Renormalization and lattice spacing equal one . . . 20

5 Quenched SU(2) QCD with adjoint fermions **21**
5.1 Setup . . . 21
5.2 Lattice Artifacts . . . 22
5.3 Mass dependence . . . 23
5.4 Finite volume artifact . . . 26
5.5 Continuum limit . . . 29
5.6 Summary . . . 31
5.7 Results . . . 31
5.8 Schwinger function . . . 33

6 Minimal Walking Technicolor **37**
6.1 Setup . . . 37
6.2 Phase transition . . . 37
6.3 $\tilde{A}$ and $\tilde{B}$ function . . . 39
6.4 Asymmetry lattice artifacts . . . 40
6.5 Finite volume artifacts . . . 41
6.6 Border of the phase transition . . . 41
6.7 Summary . . . 43
6.8 Results . . . 43
6.9 Schwinger function . . . 44

7 Conclusion and Outlook **46**

1 Introduction

To this day, the standard model(SM) of particle physics is the most successful theory which accurately describes many experimental results. Consisting of six quarks, six leptons one Higgs boson and four gauge bosons it is composed of four different sectors, namely QED, QCD , the electroweak sector and the Higgs sector.
Despite its great success, we still have not observed the Higgs boson. However there is new experimental observed particle at the LHC [1][2]. This particle has a mass of 125GeV which is a boson with yet to determine quantum numbers. For this reason this particle could be the Higgs boson. There is one result which supports this assumption [3].
Even if this new particle is the Higgs boson, we still face problems involving the SM. The most well known fact is that gravity is not part of the SM. Furthermore the dark matter is also not part of the SM. An other problem is that the observed matter-antimatter asymmetry in the universe is larger then the SM predicts. For all these reasons the SM can not fully describe nature.
In contrast to these experimental facts there are also theoretical arguments which suggest that the SM should not be able to fully describe nature. The first argument is that the Higgs sector requires to be an effective theory. An effective theory is usually described by a scale which is the upper limit for the validity of the theory. If we would remove this scale in the theory, the Higgs sector becomes trivial. An other argument is the hierarchy problem. Calculating quantum corrections to the Higgs mass we find that they depend on the cutoff squared [4]. For this reason we have to fine-tune the SM for the correct Higgs mass. There is no explanation within the SM for this effect.
Following these exemplary arguments and facts, we have to find a theory which still explains the effects and matter described by the SM and on the other hand also incorporates at least the experimental facts. Theories which try to get a step closer to such a theory are called beyond the standard model(BSM) theories. The BSM theories involve string theory, supersymmetry, technicolor, grand unifying theories, extra dimensions and many more. Some approaches try to quantize gravity while others try to overcome theoretical problems. Both approaches are reasonable despite the fact that the theoretical problems could just be features of nature. One reason for this is that usually one gets new particles which become new dark matter candidates which in turn would explain at least one experimental fact.
Focusing on the hierarchy problem there are at least two possible BSM theories which get rid of the problem: supersymmetry[5] and technicolor [4]. In this thesis we will focus on technicolor, more precisely minimal walking technicolor. Technicolor is a QCD like theory which replaces the Higgs boson with a bound state composed of techniquarks and technigluons. The minimal walking technicolor theory possess the gauge group SU(2) with two adjoint fermions. This theory is currently under investigation [6][7][8]. One important quantity for this theory is the anomalous mass dimension of the quark propagator. This is the motivation why we will calculate the quark propagator which enables us to determine this quantity directly. There are already indirect results for the anomalous mass dimension which suggest that is has to be small compared to one.[9][10][11][12][6][7][13]
Furthermore we will also consider quenched SU(2) QCD which is also the quenched minimal walking technicolor theory. Another motivation to look at this case comes from SU(3) QCD. Important properties of QCD are confinement and chiral symmetry breaking. As both stem from non-perturbative mechanisms we do not know what they are in detail and if both are connected. But we know that there is a phase transitions in QCD which restores the chiral symmetry and leads to deconfinement. Both phase transitions have their own transition temperature T_{ch} and T_{dec}. Using lattice gauge theory the relation $T_{dec} \simeq T_{ch}$ for the fundamental representation and zero baryonic potential is

found [14]. However this relation does not hold for the adjoint representation of any considered gauge groups so far. Therefore any explanation for this relation has also to explain why those temperatues does not coincide for the adjoint representation. One possible explanation is that there is a connection between confinement and chiral symmetry breaking which was investigated in [15][16][17][18][19].
As we have seen some properties of QCD changes if we change the representation. For this reason lattice calculations for adjoint fermions [20][21][22][23][24][25] are performed since nearly 30 years.

This thesis is organized as follows: Chapter two will start with the basic idea behing technicolor. Afterwards we will give a reason for walking and introduce the minimal walking technicolor. The last section is denoted to the quark propagator. In chapter three we introduce QCD.This section is followed with an introduction to lattice QCD. We conclude the chapter with the Wilson Dirac operator. In chapter four we present the methods which we use to calculate our results. In chapter five and six we will present our results for quenched SU(2) QCD and minimal walking technicolor. Both chapters start with the setup for the calculation. Following this, we take a look at the lattice artfiacts before we present the M function and the Schwinger functions. Finally we sum our results up in chapter seven and will give an outlook for possible further investigations.

2 Minimal Walking Technicolor

In this chapter we will follow the reviews [4] and[26].

Having introduced the main idea behind technicolor in the last chapter we will first introduce the dynamical electroweak symmetry breaking. Afterwards we introduce extended Technicolor theories which will lead to the idea of walking dynamics. In the end we will present the minimal walking technicolor theory and some basic properties of the quark propagator.

2.1 Electroweak Symmetry Breaking

Before we can replace the Higgs boson with techniquarks we have to recall the features of the Higgs boson. The two important features are, providing the mass for the SM fermions and to break the electroweak symmetry. At first we will concentrate on the electroweak symmetry breaking.
Looking at the SM we find that QCD also breaks the electroweak symmetry[27]. The reason for this is the condensation of the quark bilinear

$$\left\langle \overline{u}_L u_r + \overline{d}_L d_R \right\rangle \neq 0 \tag{2.1.1}$$

For this reason we get masses for the W boson even if we discard the Higgs sector. The resulting mass for the W boson would be roughly 29MeV. Comparing this result to the measured 80GeV, we see that we need an other electroweak symmetry breaking effect to get this mass right. We solve this problem in the SM by the Higgs boson. An other possibility is to add a new sector which is similar to QCD which is the original idea of technicolor. The problem to achieve the right W boson mass can be solved by increasing the scale of this new sector. For this reason, a simple technicolor theory is the scaled up QCD. One scaled up QCD theory is a non-abelian gauge theory with the gauge group $SU(N_{TC})$ and two Dirac fermions in the fundamental representation. It is important to note that we need at least two Dirac flavors to realize the symmetry $SU(2)_L \times SU(2)_R$ which is present in the SM.

2.2 Fermion masses

The Higgs boson gives the SM fermions mass trough the Yukawa terms of the form [28]

$$\overline{q^L}_i G^u_{ij} u^r_j \tag{2.2.1}$$

where q^L is the left-handed quark doublet, G^u are the Yukawa coupling matrices and u^r is the right-handed fermion singlet of an up-type-quark. From this term alone we see that we will get four-fermion operators if the Higgs is a composite particle. We can interpreted those operators as low energy operators coming from an other strongly interacting theory which emerges at even higher energies than the electroweak theory. Since there are a lot of possibilities we get again a large class of theories which are called extended technicolor(ETC) theory.
One possible model is the one family model. We use the gauge group $SU(N_{ETC})$ for the ETC dynamics. $N_{ETC} = N_{TC} + N_G$ where N_G is the number of generations in the SM. Furthermore the TC uses a complete generation of quarks and leptons. The condensation of these particles give the SM fermions their masses. The three different mass scales for the SM fermions are achieved

by three spontaneously symmetry breakings of the ETC gauge group. The model does not specify how this breaking occurs nor does it regard the breaking of the weak isospin symmetry.
Even without knowing the specific ETC we can still make some general remarks about the theory[29]. Denoting the TC particles as Q and the fermions as ψ we get the four fermion operators

$$\alpha_{ab}\frac{\overline{Q}T^aQ\overline{\psi}T^b\psi}{\Lambda^2_{ETC}}+\beta_{ab}\frac{\overline{Q}T^aQ\overline{Q}T^bQ}{\Lambda^2_{ETC}}+\gamma_{ab}\frac{\overline{\psi}T^a\psi\overline{\psi}T^b\psi}{\Lambda^2_{ETC}}+..., \tag{2.2.2}$$

where the coefficients α, β and γ parametrize the fact, that we have not yet chosen a specific ETC. Λ_{ETC} is the scale of the ETC and T includes chiral factors like $(1 \pm \gamma_5) \backslash 2$. We derive from the first term the SM fermion mass

$$m_q \approx \frac{g^2_{ETC}}{M^2_{ETC}} \left\langle \overline{Q}Q \right\rangle_{ETC} \tag{2.2.3}$$

where m_q is the mass of a SM quark, g_{ETC} is the ETC coupling constant evaluated at the ETC scale, M_{ETC} is the mass of an ETC gauge boson and $\left\langle \overline{Q}Q \right\rangle_{ETC}$ is the TC condensate evaluated at the ETC scale. From the second term in (2.2.2) we derive the masses of Goldstone bosons and techniaxions [29]. The third therm in (2.2.2) provide flavor changing neutral currents(FCNCs). Assuming that γ_{ab} is of the order one(which is a naive assumption) and including experimental results provides us with a constraint to the ETC scale. We find that this scale has to be 10^3 TeV or even larger [30]. Using this scale we can deduce a naive estimate for the largest possible mass in a QCD-like Theory. We find this to be roughly 100MeV which is below the top quark mass.

2.3 Walking

It is apparent that we have to change our QCD-like theory to explain the top quark mass. To better understand how we should change the theory we have to analyze the TC condensate. Using the renormalization group we find

$$\left\langle \overline{Q}Q \right\rangle_{ETC} = exp\left(\int_{\Lambda_{TC}}^{\Lambda_{ETC}} d\left(ln\mu\right)\gamma_m\left(\alpha\left(\mu\right)\right)\right)\left\langle \overline{Q}Q \right\rangle_{TC} \tag{2.3.1}$$

where γ_m is the anomalous dimension of the techniquark mass-operator and $\alpha\left(\mu\right)$ is the running coupling. If we assume this running coupling behaves like the one in QCD we can compute the integral and get

$$\left\langle \overline{Q}Q \right\rangle_{ETC} \sim ln\left(\frac{\Lambda_{ETC}}{\Lambda_{TC}}\right)^{\gamma_m}\left\langle \overline{Q}Q \right\rangle_{TC} \tag{2.3.2}$$

Assuming the ratio is not too large we can neglect the logarithmic factor and use directly the condensate evaluated at the TC scale. We get for the fermion masses

$$m_q \approx \frac{g^2_{ETC}}{M^2_{ETC}}\Lambda^3_{TC}, \quad \left\langle \overline{Q}Q \right\rangle_{TC} \sim \Lambda^3_{TC} \tag{2.3.3}$$

So far we still have used QCD like dynamics. Now we change this fact by introducing walking. Walking is a kind of dynamics which is defined by the fact the the TC coupling does not run to the

UV fix-point. Instead the coupling has a near conformal fix-point which leads to an enhancement of the TC condensate

$$\langle \overline{Q}Q \rangle_{ETC} \sim \left(\frac{\Lambda_{ETC}}{\Lambda_{TC}} \right)^{\gamma_m(\alpha^*)} \langle \overline{Q}Q \rangle_{TC} \tag{2.3.4}$$

where α^* is the near conformal fixed point. Assuming that γ is of the order one we get a much larger contribution to our condensate. Looking back at the four-fermion operators in (2.2.2) we see that the terms involving the TC particles are enhanced by the factor $\left(\frac{\Lambda_{ETC}}{\Lambda_{TC}}\right)^{\gamma_m(\alpha^*)}$. Since we did not enhanced the term responsible for the FCNCs, this new dynamics help to resolve this problem. We want to stress that walking is not the only solution to resolve the problems which a QCD like theory face.

2.4 Minimal Walking Technicolor

Having introduce the basics, we want introduce the TC model which we consider in this thesis, namely the Minimal Walking Technicolor(MWT) model. The MWT features two fermions and one technigluon in the adjoint representation. Furthermore it has walking dynamics. These two elements give the model the name because there is no possibility to have less matter in the TC section if we have walking dynamics. Despite this new TC matter we also have to add a new generation of Dirac leptons whose left handed components form a weak doublet. The reason for this unexpected addition to the SM is the Witten anomaly [31].
We see that this model has new particles coming from the TC sector

$$Q_L^a = \begin{pmatrix} U^a \\ D^a \end{pmatrix}_L,\ U_R^a,\ D_R^a, \quad a = 1,2,3 \tag{2.4.1}$$

where a is the adjoint color index of SU(2) and new leptons

$$L_L = \begin{pmatrix} N \\ E \end{pmatrix}_L,\ N_R,\ E_R. \tag{2.4.2}$$

The TC particles form the condensate $\langle \overline{U}U + \overline{D}D \rangle$ which breaks the electroweak symmetry as described beforehand. To cancel the gauge anomalies we assign the hypercharge as

$$\begin{aligned} Y(Q_L) = \frac{y}{2}, \qquad & Y(U_R, D_R) = \left(\frac{y+1}{2}, \frac{y-1}{2} \right) \\ Y(L_L) = -3\frac{y}{2}, \qquad & Y(N_R, E_R) = \left(\frac{-3y+1}{2}, \frac{-3y-1}{2} \right) \end{aligned} \tag{2.4.3}$$

where it is possible to chose an arbitrary real value for y [32]. Furthermore we find that the electric charge is $Q = T^3 + Y$, where T^3 is the weak isospin generator. To recover the SM hypercharge we have to set $y = \frac{1}{3}$.

We conclude this model with the new Lagrangian for the Higgs sector

$$\mathcal{L} \to \frac{1}{4}F^a_{\mu\nu}F^{a\mu\nu} + i\overline{Q}_L\gamma^\mu D_\mu Q_L + i\overline{U}_R\gamma^\mu D_\mu U_R + i\overline{D}_R\gamma_\mu D_\mu D_R + \tag{2.4.4}$$
$$+i\overline{L}_L\gamma^\mu D_\mu L_L + i\overline{E}_R\gamma^\mu D_\mu E_R + i\overline{N}_R\gamma^\mu D_\mu N_R$$

$$F^a_{\mu\nu} = \partial_\mu A^a_\nu - \partial_\nu A^a_\mu + g_{TC}\epsilon^{abc}A^b_\mu A^c_\nu \tag{2.4.5}$$

$$D_\mu Q^a_L = \left(\delta^{ac}\partial_\mu + g_{TC}A^b_\mu\epsilon^{abc} - i\frac{g}{2}\overrightarrow{W}_\mu\cdot\overrightarrow{\tau}\delta^{ac} - ig'Y\left(Q_L\right)B_\mu\delta^{ac}\right)Q^c_L \tag{2.4.6}$$

$$D_\mu Q^a_R = \left(\delta^{ac}\partial_\mu + g_{TC}A^b_\mu\epsilon^{abc} - ig'Y\left(Q_R\right)B_\mu\delta^{ac}\right)Q^c_R \tag{2.4.7}$$

$$D_\mu L^a_L = \left(\delta^{ac}\partial_\mu - i\frac{g}{2}\overrightarrow{W}_\mu\cdot\overrightarrow{\tau}\delta^{ac} - ig'Y\left(L_L\right)B_\mu\delta^{ac}\right)L^c_L \tag{2.4.8}$$

$$D_\mu L^a_R = \left(\delta^{ac}\partial_\mu - ig'Y\left(L_R\right)B_\mu\delta^{ac}\right)L^c_R \tag{2.4.9}$$

where a,b,c=1,2,3 .A_ν are the techni gauge bosons, W_μ are the gauge boson associated to $SU(2)_L$ and B_μ is the gauge boson associated to the hypercharge. γ^μ are the gamma matrices (see section 3.2), t^a are the Pauli matrices and ϵ^abc is the fully antisymmetric symbol.

2.5 Quark Propagator

After introducing the MWT it is apparent that the anomalous dimension of the quark propagator is important for the phenomenology of the model. For this reason we will calculate the quark propagator and derive this quantity. The quark propagator is a gauge dependent two point function. Therefore it is important to chose a gauge. We have chosen Landau gauge which is defined by

$$\partial_\mu A_\mu\left(x\right) \tag{2.5.1}$$

More precisely we have chosen minimal Landau gauge because we encounter the Gribov ambiguity in the non perturbative regime [33]. The main reason to chose this specific gauge is that the tensor structure of the quark propagator is [35]

$$S^{-1}\left(p\right) = -iA\not{p} + B\left(p\right) \tag{2.5.2}$$

where $S^{-1}\left(p\right)$ is the inverse of the propagator and $A\left(p\right)$ and $B\left(p\right)$ are some yet to determine functions. We can use these two functions to define the M function

$$M\left(p\right) = \frac{A\left(p\right)}{B\left(p\right)} \tag{2.5.3}$$

This quantity is in one loop order [34]

$$M\left(p^2\right) = M\left(\mu\right)\left(\omega\log\left(\frac{p^2}{\mu^2}\right) + 1\right)^{-\gamma} \tag{2.5.4}$$

where μ is the renormalization point. Knowing all this we can determine directly the anomalous mass dimension γ from the quark propagator.

3 QCD on the lattice

In this chapter we follow [36], [37] and [38],
As both, QCD and Technicolor, are strongly interacting theories, we will first introduce the basic properties of theses theories, using QCD as an example. After this we will introduce the lattice and formulate a discretized version of the QCD action. Afterwards we derive the Dirac operator on the lattice from this action. Discussing this operator we see that we have to add the Wilson term which leads to the Wilson Dirac operator

3.1 Strongly interacting field theories

QCD is the theory of quarks and gluons. Quarks are the basic matter fields and gluons are spin one fields which mediate the interaction between the quarks. Like the electromagnetic force QCD also has charges. For quarks we have the color charges red, blue and green and their respective anti-colors while gluons have 8 different colors but no anti-colors. Furthermore we can not observe a single color. For this reason every physical object has to be neutral according to these charges. For quarks we achieve this by combining all three different colors or a color and the respective anti-color. On the other hand for gluons we just have to combine two different colors. This results in the effect that there are actually physical objects possible which consist only of gluons.
After this basic phenomenological introduction, we introduce the theoretical description of the theory. In QCD the fermions are described by Dirac 4-spinors

$$\psi_\alpha^f(x)_a, \overline{\psi}_\alpha^f(x)_a \tag{3.1.1}$$

These fields have two different indices, namely the Dirac index α and the color index c. x is the space-time position. In QCD we have $\alpha = 1,2,3,4$ and $c = 1,2,3$. The flavor index f distinguish between different mater fields like up and down. ψ and $\overline{\psi}$ are connected by $\overline{\psi} = \psi^\dagger \gamma_0$, where γ_0 is the gamma matrix related to the time.
QCD is a gauge theory, therefore there are also gauge fields

$$A_\mu(x)_{cd} \tag{3.1.2}$$

The new index d is also a color index and μ is a Lorentz index which denotes the different space-time directions. The color indices in the gauge fields comes from the incorporation of a Lie group into the theory

$$A_\mu = A_\mu^a \tau_a \tag{3.1.3}$$

with the generators τ_a in a representation of the algebra. Such gauge theories are generally called Yang-Mills theory. In our case, we have $SU(3)/Z_3$ and the fundamental representation for the generators. For any gauge theory, there is a gauge transformation $G = exp(ig\tau^a \omega_a(x))$ which infinitesimal reads as

$$A_\mu^a \to A_\mu^a + D_\mu^{ab}\omega_b \tag{3.1.4}$$

$$D_\mu^{ab} = \delta^{ab}\partial_\mu - g f_c^{ab} A_\mu^c \tag{3.1.5}$$

$$\psi_i \to (G\psi)_i = G_{ij}\psi_j = exp(-ig\tau^a\omega_a)_{ij}\psi_j \tag{3.1.6}$$

where f_c^{ab} are the structure constants for the Lie algebra and $w(x)^a$ is the gauge transformation function. The constant g is the coupling constant for the Yang-Mills theory. The next step is to incorporate this into the covariant derivative

$$(D_\mu)_{ij} = \delta_{ij}\partial_\mu + igA_\mu^a (\tau_a)_{ij} \tag{3.1.7}$$

The last step is to construct a gauge-invariant action. It turns out that $tr(F_{\mu\nu}F^{\mu\nu}) = F_{\mu\nu}^a F_a^{\mu\nu}$ is gauge-invariant for $F_{\mu\nu} = \partial_\mu A_\nu - \partial_\nu A_\mu - ig[A_\mu, A_\nu] = F_{\mu\nu}^a$. Finally we combine all these into the Lagrangian of QCD

$$\mathcal{L}_{QCD} = -\frac{a}{4}F_{\mu\nu}^a F_a^{\mu\nu} + \sum_f \overline{\psi}_i^f \left(i\gamma^\mu D_\mu^{ij} - m_f\delta^{ij}\right)\psi_j^f \tag{3.1.8}$$

where γ^μ are the gamma matrices (see section 3.2). We arrive at the gauge invariant action

$$S_{QCD}[A_\mu] = \int d^d \mathcal{L}_{QCD}[A_\mu] \tag{3.1.9}$$

where d is the dimension of the spacetime, in our case 3+1, which means we have one time direction and three space directions.

3.2 Euclidean space

In the last section we introduced the action S_{QCD}. With this action we can calculate any observable through the path integral

$$< O_2(t)\, O_1(0) >= \int \mathcal{D}[A_\mu]\, O_2[A_\mu(x_0 = t)]\, O_1[A_\mu(x_0 = 0)]\, e^{iS[A_\mu]} \tag{3.2.1}$$

$$\mathcal{D}[A_\mu] = \prod dA_\mu(x) \tag{3.2.2}$$

where O_1 and O_2 are the observables and x_0 is the time direction. The Integral over $\mathcal{D}[A_\mu]$ means we have to calculate over all possible field configurations A_μ at any point. For details for this prescription see for example [37] Unfortunately this expression gives us a problem. We have to integrate over all possible field configurations while we can not be sure which of these give us the main contribution to our observable. To circumvent this problem, we change our metric. In quantum field theory we have usually a Minkowski space which means the metric is $\eta_{\mu\nu} = Diag(-1, 1, 1, 1)$. Now we transform the time $x_0 \to ix_0$. This changes the metric to the matrix of unity, but we have imaginary time. Therefore we have to use the wick rotation(see for example[39]) to get back to a real time. After this procedure our path integrals changes to

$$< O_2(t)\, O_1(0) >= \int \mathcal{D}[A_\mu]\, O_2[A_\mu(x_0 = t)]\, O_1[A_\mu(x_0 = 0)]\, e^{-S_E[A_\mu]} \tag{3.2.3}$$

where S_E is the euclidean action. We see the phase factor changed into a real exponential function. Therefore we can interpret this function as a weight factor from a distribution if we divide it by a normalization factor. This weight factor tells us how a configuration $A_\mu(x)$ contributes to the expectation value. On the other hand it allows us to apply algorithms and methods from statistical mechanics to solve our problems. For example to calculate an expectation value we just have to

create configurations which are distributed according to the distribution given by the weight factor. After this we calculate the observable for each configuration. The mean value of this calculation is the expectation value of the observable. This was done in this thesis.

We have introduced euclidean spacetime. This has another consequence, we get new gamma matrices because the commutator

$$\{\gamma_\mu, \gamma_\nu\} = \eta_{\mu\nu} \tag{3.2.4}$$

depends on the metric. Therefore we have to determine them for euclidean spacetime. In this thesis we use the following gamma matrices

$$\gamma_1 = \begin{pmatrix} 0 & 0 & 0 & -i \\ 0 & 0 & -i & 0 \\ 0 & i & 0 & 0 \\ i & 0 & 0 & 0 \end{pmatrix}, \quad \gamma_2 = \begin{pmatrix} 0 & 0 & 0 & -1 \\ 0 & 0 & 1 & 0 \\ 0 & 1 & 0 & 0 \\ -1 & 0 & 0 & 0 \end{pmatrix} \tag{3.2.5}$$
$$\gamma_3 = \begin{pmatrix} 0 & 0 & -i & 0 \\ 0 & 0 & 0 & i \\ i & 0 & 0 & 0 \\ 0 & -i & 0 & 0 \end{pmatrix}, \quad \gamma_4 = \begin{pmatrix} 0 & 0 & 1 & 0 \\ 0 & 0 & 0 & 1 \\ 1 & 0 & 0 & 0 \\ 0 & 1 & 0 & 0 \end{pmatrix}$$

3.3 Introducing the lattice

The calculation of a value can be performed either with analytical methods or with the computer. In this thesis we use the later. We introduce a lattice Λ which will give us a natural regulator, namely the lattice spacing. Any point x_{lat} in the lattice has the form

$$x = (n_1, n_2, n_3, n_4), \quad n_i \in \{1, ..., N_i\}, \ i = 1, 2, 3, 4 \tag{3.3.1}$$

N_i is the number of points in the direction i. The connection with the continuous spacetime is made through $x_{phys} = a * x_{lat}$. a is the lattice spacing. It is possible to chose different lattice spacings for the different directions but we have used just one lattice spacing for every direction. For $a \to 0$, we get back to the continuous case but our spacetime volume would become zero. Therefore we have always to study the case $a \to 0$ for $V = a \prod_{i=1}^{4} N_i = const.$
The next step is to discretize the action. The first problem is to replace the derivative with a term which becomes the derivative in the limit $a \to 0$. Such a term is already known by the definition of the derivative

$$f'(x) = \lim_{\epsilon \to 0} \frac{f(x+\epsilon) - f(x)}{\epsilon} \tag{3.3.2}$$

Looking at the Taylor series for the function $f(x \pm \epsilon) = f(x) \pm \epsilon f'(x) + \epsilon^2 f''(x) + \mathcal{O}(\epsilon^3)$ we can determine the error and find an other possible term

$$\frac{f(x+\epsilon) - f(x)}{\epsilon} = f'(x) + \mathcal{O}(\epsilon) \tag{3.3.3}$$
$$\frac{f(x+\epsilon) - f(x-\epsilon)}{2\epsilon} = f'(x) + \mathcal{O}(\epsilon^2) \tag{3.3.4}$$

The first term is called derivative with forward differences while the second is called derivative with central differences. Setting $\epsilon = a$, we see the error for the later reduces faster than the first one. Therefore it is more advantageous to use it in the action for the lattice.
The next problem is to replace the integral. Here we use again the mathematical definition of the integral. On possible formula is

$$\int_a^b f(x)\,dx = \lim_{n\to\infty} \sum_{i=1}^{n-1} (x_{i+1} - x_i) * f(x_i) \tag{3.3.5}$$

$$x_1 = a,\ x_n = b,\ x \in (a,b)\,,\ x_{i+1} > x_i \tag{3.3.6}$$

which is correct if the function is integrable. Since we expect that any Lagrangian in our action is integrable, we found a way to replace this integral on the lattice by a sum

$$\int f(x)\,d^d x \to a^4 \sum_{x\in\Lambda} f(x) \tag{3.3.7}$$

Finally we can now convert our action (3.1.9) to the lattice. In this process we drop the gauge fields which gives us the free fermion action

$$S_F^0\left[\psi,\overline{\psi}\right] = a^4 \sum_{x\in\Lambda} \overline{\psi}(x) \left(\sum_{\mu=1}^{4} \gamma_\mu \frac{\psi(x+\widehat{\mu}) - \psi(x-\widehat{\mu})}{2a} + m\psi(x) \right) \tag{3.3.8}$$

where $\widehat{\mu}$ is the vector of unity in the direction μ which means for $x = (x_1, x_2, x_3, x_4)$ it acts as $x + \widehat{1} = (x_1 + 1, x_2, x_3, x_4)$. Therefore it is possible to get points which would be outside of the lattice, for example $(N_x, 0, 0, 0) + (1, 0, 0, 0) = (N_x + 1, 0, 0, 0)$. To solve this problem, we use periodic boundaries

$$x_\mu = n + N_\mu = n \tag{3.3.9}$$

Later we will introduce a anti-periodic boundary which will not change the discussion in the next chapters.

3.4 Link variables

In the last section we introduced the free fermion action on the lattice. We now examine the transformation under a gauge transformation. In chapter 1.1 we introduced the gauge transformation $G = exp(iw_a\tau^a)$, with t^a in the gauge algebra SU(3). The algebra SU(3) consists of traceless Hermitian 3×3 matrices. If we combine this with the formula

$$\left(e^M\right)^\dagger = e^{M^\dagger} \tag{3.4.1}$$

which we get if we combine the definition of the exponential function and the properties of the adjoint, we get for any $\Omega(n) \in G$

$$\Omega^\dagger(n) = \Omega^{-1}(n) \tag{3.4.2}$$

Lets reconsider the transformation rules for the fermion field, incorporating the new knowledge,

$$\psi(n) \to \psi'(n) = \Omega(n)\,\psi(n) \quad , \quad \overline{\psi}(n) \to \overline{\psi}'(n) = \overline{\psi}(n)\,\Omega^\dagger(n) \tag{3.4.3}$$

We see from this formula that the mass term $\overline{\psi}(n) m\psi(n)$ is gauge invariant. This coincide with the continuum case. But the other term $\overline{\psi}(n)\psi(n+\widehat{\mu})$ is not gauge invariant because $\Omega^{\dagger}(n)\Omega(n+\widehat{\mu}) \neq 1$ in general. Therefore we introduce a new field $U_{\mu}(n)$ which transforms according to

$$U_{\mu}(n) \to U'_{\mu}(n) = \Omega(n) U_{\mu}(n) \Omega^{\dagger}(n+\widehat{\mu}) \tag{3.4.4}$$

and change the term in the action

$$\overline{\psi}(n)\psi(n+\widehat{\mu}) \to \overline{\psi}(n) U_{\mu}(n)\psi(n+\widehat{\mu}) \tag{3.4.5}$$

Using the transformation formulas we see that the new term is gauge invariant. We demand that the new field $U_{\mu}(n)$ lies in the gauge group S(U3). Furthermore it carries a directional index μ. Therefore there are eight fields on every lattice point attached to the links of the lattice. Those fields are called link variables. Having only introduce link variables pointing in positive direction, we introduce those pointing in negative direction by doing the same as before for the term $\overline{\psi}(n)\psi(n-\widehat{\mu})$. We get the following transformation

$$U_{-\mu}(n) \to U'_{\mu}(n) = \Omega(n) U_{\mu}(n) \Omega^{\dagger}(n-\widehat{\mu}) \tag{3.4.6}$$

Comparing this with the result for the positive direction we get

$$U_{-\mu}(n) = U^{\dagger}_{\mu}(n-\widehat{\mu}) \tag{3.4.7}$$

which connects link variables living on the same link witch different base points. Since the base point is irrelevant, the value depends only on the link in the lattice hence the name link variable. With these new fields we construct a new gauge invariant action the so-called naive fermion action for fermion in the external field U.

$$S_F\left[\psi,\overline{\psi},U\right] = a^4 \sum_{n\in\Lambda} \overline{\psi}(n) \left(\sum_{\mu=1}^{4} \gamma_{\mu} \frac{U_{\mu}(n)\psi(n+\widehat{\mu}) - U_{-\mu}(n)\psi(n-\widehat{\mu})}{2a} + m\psi(n) \right) \tag{3.4.8}$$

After this we have to check if the new action becomes the continuum action for $a \to 0$ as we demanded for the objects in chapter 1.3. We see that the mass term is already the one from the continuum. Therefore we just have to care for the first term. There we encounter our new fields. Since we only know their transformation rules we have to investigate those fields further.
We already know the transformation rules (3.4.4) and (3.4.6). In the continuum there is also an object with these transformation rules. It is the path-ordered exponential integral of the gauge field A_{μ} along some Curve $\mathcal{C}_{xy}$ connecting two points x and y, the so-called gauge transporter:

$$G(x,y) = P\ exp\left(\int_{\mathcal{C}_{xy}} A ds \right) \tag{3.4.9}$$

The gauge transformation

$$G(x,y)) \to \Omega(x) G(x,y)) \Omega^{\dagger}(y)) \tag{3.4.10}$$

is the same as for the link variables if $x = n$ and $y = n+\widehat{\mu}$. Therefore we interpret the link variables as the lattice version of the gauge transporter. Now we introduce algebra-valued gauge fields $A_{\mu}(x)$

and approximate the integral in the exponent by $lA_\mu(x)$, where l is the length of the path. This approximation has an error of the order l. In this approximation the path orderings is not necessary anymore. Using these approximations we identify the link variables as

$$U_\mu(n) = exp(iaA_\mu(n)) \tag{3.4.11}$$

With this new expression for the link variables we can now discuss the continuum limit for the action (3.4.8). We insert the expansion for (3.4.11)

$$U_\mu(n) = 1 + iaA_\mu(n) + \mathcal{O}(a^2) \tag{3.4.12}$$

into the naive fermion action and get

$$S_F\left[\psi,\overline{\psi},U\right] = S_F^0\left[\psi,\overline{\psi},U\right] + S_F^I\left[\psi,\overline{\psi},A\right] \tag{3.4.13}$$

where S_F^0 is the free part as defined in (3.3.8) and S_F^I is the interaction part which is

$$\begin{aligned} S_F^I\left[\psi,\overline{\psi},A\right] &= ia^4 \sum_{n\in\Lambda}\sum_{\mu=1}^{4} \overline{\psi}(n)\gamma_\mu \frac{1}{2}\left(A_\mu(n)\psi(n+\widehat{\mu}) + A_\mu(n-\widehat{\mu})\psi(n-\widehat{\mu})\right) \\ &= ia^4 \sum_{n\in\Lambda}\sum_{\mu=1}^{4} \overline{\psi}(n)\gamma_\mu A_\mu(n)\psi(n) + \mathcal{O}(a) \end{aligned} \tag{3.4.14}$$

where we used $\psi(n\pm\widehat{\mu}) = \psi(n) + \mathcal{O}(a)$ and $A_\mu(n-\widehat{\mu}) = A_\mu(n) + \mathcal{O}(a)$. Taking again the continuum limit $a \to 0$ we arrive at the continuum action.

3.5 Dirac Propagator

In the last section we introduced the naive fermion action. Now we derive the main object in this thesis, the Dirac operator. For this we write the naive fermion action with all indices

$$\begin{aligned} S_F\left[\psi,\overline{\psi},U\right] &= a^4 \sum_{a,b,\alpha,\beta}\sum_{n\in\Lambda} \overline{\psi}_\alpha(n)_a \times \\ \times\left(\sum_{\mu=1}^{4}(\gamma_\mu)_{\alpha\beta}\frac{U_\mu(n)_{ab}\,\psi_\beta(n+\widehat{\mu})_b - U_{-\mu}(n)_{ab}\,\psi_\beta(n-\widehat{\mu})_b}{2a} + m\delta_{ab}\delta_{\alpha\beta}\psi_\beta(n)_b\right) \end{aligned} \tag{3.5.1}$$

We can rewrite this term as

$$S_F\left[\psi,\overline{\psi},U\right] = a^4 \sum_{a,b,\alpha,\beta}\sum_{n,m\in\Lambda} \overline{\psi}_\alpha(n)_a\, D_{\alpha\beta}(n|m)_{ab}\,\psi_\beta(n)_b \tag{3.5.2}$$

$$D_{\alpha\beta}(n|m)_{ab} = \sum_{\mu=1}^{4}(\gamma_\mu)_{\alpha\beta}\frac{U_\mu(n)_{ab}\,\delta_{n+\widehat{\mu},m} - U_{-\mu}(n)_{ab}\,\delta_{n-\widehat{\mu},m}}{2a} + m\delta_{ab}\delta_{\alpha\beta}\delta_{n,m} \tag{3.5.3}$$

with D as the naive Dirac operator. Let us discuss this operator further. As a first step we only consider the free case , $U_\mu(n) = 1$. We want to calculate the mass spectrum of this operator but a

direct inversion is not possible. Therefore, as a first step, we compute a Fourier transformation on the lattice [36].

$$\tilde{D}(p|q) = \frac{1}{|\Lambda|} \sum_{n,m\in\Lambda} e^{-ipna} D(n|m) e^{iqma} = \delta(p-q)\tilde{D}(p) \tag{3.5.4}$$

$$\tilde{D}(p) = m1 + \frac{i}{a}\sum_{\mu=1}^{4} \gamma_\mu \sin(p_\mu a) \tag{3.5.5}$$

where $|\Lambda|$ is the total number of points of the lattice. We see that the Fourier transformed Dirac operator is nonzero for $p = q$. That is why we will consider only the object $\tilde{D}(p)$ in the following part of the thesis. Furthermore the lattice the momenta in the Fourier transformation are

$$p_\mu = 2\pi\frac{k}{aN_\mu}, \quad k \in 0, 1, 2, ..., N_\mu - 1 \tag{3.5.6}$$

We see that the argument of the sinus is independent of the lattice spacing. This will become important later on.
After we calculated the Fourier transform we have to invert this expression. This can be done directly and we get

$$\tilde{D}^{-1}(p) = \frac{m1 - \frac{i}{a}\sum_{\mu=1}^{4}\gamma_\mu \sin(p+\mu a)}{m^2 + \frac{1}{a^2}\sum_{\mu=1}^{4}\sin(p_\mu a)^2} \tag{3.5.7}$$

The last step is to perform a Fourier transformation again

$$D^{-1}(n|m) = \frac{1}{|\Lambda|}\sum_{p\in\tilde{\Lambda}} \tilde{D}^{-1}(p) e^{ip(n-m)a} \tag{3.5.8}$$

This operator is called quark propagator. In the following part of the thesis the term quark propagator refers to the expression $\tilde{S}(p) = \tilde{D}^{-1}(p)$. Considering now only massless fermions we see that

$$\tilde{S}(p)\Big|_{m=0} = \frac{-\frac{i}{a}\sum_{\mu=1}^{4}\gamma_\mu \sin(p+\mu a)}{\frac{1}{a^2}\sum_{\mu=1}^{4}\sin(p_\mu a)^2} \xrightarrow{a\to 0} \frac{-i\sum_{\mu=1}^{4}\gamma_\mu p_\mu}{p^2} \tag{3.5.9}$$

we get the correct naive continuum limit with the pole $p = 0$. This means the Dirac operator describes a massless free fermion in the continuum which we expected, since we considered free massless fermions in the first place. This situation changes on the lattice. We get additional poles because $\sin\left(\frac{\pi}{a}\right)$ is also zero. As a result we get 15 extra poles, so-called doublers, which do not appear in the continuum. The next step is therefore to remove these unwanted poles. We achieve this by adding an additional term to the naive Dirac operator

$$\tilde{D}(p) = m1 + \frac{i}{a}\sum_{\mu=1}^{4}\gamma_\mu \sin(p_\mu a) + \frac{1}{a}\sum_{\mu=1}^{4}(1 - \cos(p_\mu a)) \tag{3.5.10}$$

The new term is called Wilson term. This term vanishes for $p = 0$ and raises the mass if a momentum component is equal to $\frac{\pi}{a}$. Calculating the new mass for the doublers we get

$$m + \frac{2l}{a} \tag{3.5.11}$$

where l is the number of momentum components which are equal to $\frac{\pi}{a}$. In the continuum limit,$a \to 0$ the mass goes to infinity and decouples from the theory. Calculating the new quark propagator $S(p)$ also shows that the unwanted poles are gone. The last thing to do is to calculate the new Dirac operator $D(n|m)$ through a Fourier transformation. The result is

$$D_{\alpha\beta}(n|m)_{ab} = -\sum_{\mu=\pm 1}^{\pm 4} (1-\gamma_\mu)_{\alpha\beta} \frac{U_\mu(n)_{ab}\,\delta_{n+\widehat{\mu},m}}{2a} + \left(m + \frac{4}{a}\right)\delta_{ab}\delta_{\alpha\beta}\delta_{n,m} \tag{3.5.12}$$

where we use the following definitions

$$\gamma_{-\mu} = -\gamma_\mu, \quad \mu = 1,2,3,4 \tag{3.5.13}$$

This is the Wilson Dirac operator which we will use in this thesis. The fermions are accordingly called Wilson fermions.

4 Methods

In this chapter we will introduce the necessary methods to calculate our results. We start with the quenched approximation which is important for chapter five. Following this section we will introduce unphysical states and the Schwinger function. Afterwards we introduce antiperiodic boundaries before we focus on the A,B and M function and will introduce the tree level corrections. We conclude this chapter with the used renormalization sheme and a short discussion about the Dirac operator with $a = 1$.

4.1 The quenched approximation

Before we can explain the quenched approximation we have to look at first at for example the meson propagator [34]

$$\left\langle O_T(n)\,\overline{O}_T(m)\right\rangle = -\frac{1}{Z}\int \mathcal{D}[U]\,e^{-S_G[U]}det[D_u]\,det[D_d]\,tr\left[\Gamma D_u^{-1}(n|m)\,\Gamma D_d^{-1}(m|n)\right] \tag{4.1.1}$$

$$Z = \int \mathcal{D}[U]\,e^{-S_G[U]}det[D_u]\,det[D_d] \tag{4.1.2}$$

where the meson is composed of two quark flavors. Γ is a matrix composed of one or two gamma matrices or the matrix of unity.D is the Dirac operator. Looking at the formula we find that we have to calculate two fermion determinants. These determinants are sums over closed fermion loops[34]. The definition of the quenched approximation is to set these determinants equal to unity. This means we disregard the fermion loops in the Feynman diagrams. An other part of this approximation is the construction of configurations. Instead of using the full theory to create them we just use a pure gauge theory. For these reason this approximation greatly reduces the calculation time. Despite being an approximation, this approach is capable of determining the ground states spectrum of the hadrons with light quarks.[34]

4.2 Unphysical particles and the Schwinger function

As we mentioned in section (3.1) we can not observe quarks even though they are part of QCD. This example shows that there are states which we can not observe. For this reason we can divide these states in physical and unphysical states. Physical states can be observed while we can not observe unphysical states. This splitting give rise to a new problem: we have to find a tool to tell apart these states.
Thinking about perturbation theory we have the BRST (Becchi, Rouet, Stora and Tyutin) symmetry [34]. This symmetry introduce a new operator Q where $Q\phi$ is the BRST transformation of the field ϕ. It turns out that Q is nilpotent $Q^2 = 0$. Using this new operator we can divide our space of states into three subspace H_0, H_1 and H_2. H_1 is the subspace of states which are not annihilated by Q. H_2 is the space of states which we can get by applying Q on a state in H_1. The remaining states belong to H_0 which are states annihilated by Q but are not in H_2. It can be shown that the physical subspace is the union of H_2 and H_0 [37].
With the BRST we have found a tool to identify physical states in perturbation theory. Since we use the lattice to calculate our results we have to find a non-perturbative tool. This can be achieved by expanding the approach of the BRST into the non-perturbative theory. [47]

An other way to decide where or not a state is unphysical is the positivity violation. Looking at a state

$$\psi = \int d^4x f(x) A_\mu(x) |0\rangle \tag{4.2.1}$$

where A_μ is an operator which creates the state from the vacuum $|0\rangle$ with the weight function $f(x)$. The norm of this stats is given by

$$|\psi|^2 = \int d^4x dy^4 f(x) \left\langle A_\mu^\dagger(y) A_\mu(x) \right\rangle f^\dagger(y) = \int d^4x dy^4 f(x) \Delta(x,y) f^\dagger(y) \tag{4.2.2}$$

where $\Delta(x,y) = \left\langle A_\mu^\dagger(y) A_\mu(x) \right\rangle$ is the propagator. We see if the propagator is negative for a certain degree of freedom μ we can get a negative norm for certain weight functions. If we want to ensure the probability interpretation of the theory this is forbidden for physical particles. Therefore this positivity violation is a criterion to find unphysical states.
Since we have an euclidean quantum field theory we have to change this positivity violation into the reflection positivity of the Osterwalder-Schrader axiom [48]. Focusing solely on the propagator $\Delta(x-y)$ we get the condition [40]

$$\int_0^\infty dt dt' \overline{f}(t', \overrightarrow{p}) \Delta(-(t+t'), \overrightarrow{p}) f(t, \overrightarrow{p}) \geq 0 \tag{4.2.3}$$

where $f(t, \overrightarrow{p})$ is a test function. If $\Delta(t_0, \overrightarrow{p}) < 0$ for a region around t_0, we can find a test function which violates this condition. For this reason we can enforce a condition upon the Schwinger function $\Delta(t)$

$$\Delta(t) = \frac{1}{\pi} \int_0^\infty dp_4 \cos(tp_4) \sigma\left(p_4^2\right) \geq 0 \tag{4.2.4}$$

where we have used the special case $\overrightarrow{p} = 0$ which we realized in this thesis. $\sigma\left(p_4^2\right)$ is a scalar function derived from the propagator

$$S(p) = i\not{p}\sigma_\nu\left(p^2\right) + \sigma_s\left(p^2\right) \tag{4.2.5}$$

Using the A and M function(see section 2.5) we find the following identities.

$$\sigma_\nu\left(p^2\right) = \frac{A^{-1}\left(p^2\right)}{p^2 + M^2\left(p^2\right)} \tag{4.2.6}$$

$$\sigma_s\left(p^2\right) = \frac{A^{-1}\left(p^2\right) M\left(p^2\right)}{p^2 + M^2\left(p^2\right)} \tag{4.2.7}$$

With this we can calculate the Schwinger function on the lattice which tells us if a particle is unphysical. Despite this information it is also possible to get the particle mass from this function[40]. Assuming

$$\sigma\left(p_4^2\right) = \frac{1}{p^+ m^2} \tag{4.2.8}$$

we get

$$\Delta(t) \sim e^{-mt} \tag{4.2.9}$$

Therefore we can determine the mass of a particle if the propagator has the right behaviour.

4.3 Antiperiodic boundaries

In the simulation we have antiperiodic boundaries in the time direction. To regard this, we discuss this problem in one dimension which we can later adopt for the 3+1 dimensional case. We will follow [38].
We consider an one-dimensional lattice with periodic or anti-periodic boundary and length L.We begin with the definition of the different boundary conditions

$$S\left(N_x+1\right)) = \left(-1\right)^k S\left(1\right) \tag{4.3.1}$$

$$S\left(1-1\right)) = \left(-1\right)^k S\left(N_x\right) \tag{4.3.2}$$

where $S\left(x\right)$ is the propagator on the lattice and N_x is the number of points on the lattice. The exponent k is one for anti-periodic boundary and zero for periodic boundary. Furthermore the points $x=0$ and $x=N_x$ are the same on the lattice. This definition is sufficient for the propagator defined in (3.5.10) because $S\left(x \pm n\right) = 0 \; for \; n \in \{2,3,...,N_x-1\}$. If this is not the case we had to expand this definition analog by replacing ± 1 by $\pm n, \; n \in \{2,3,...,N_x-1\}$ keeping in mind (3.3.9). By definition the propagator S has the following property:

$$\sum_n S(m|n)D(n|l) = \delta_{ml} \tag{4.3.3}$$

The propagator is a translation invariant function. Therefore we can write it as

$$S(m|n) = S(m-n) = \frac{1}{L}\sum_p e^{ip(m-n)}\tilde{S(p)} \tag{4.3.4}$$

If we combine these equations we get for the momentum p the following conditions

$$p = \begin{cases} \frac{2\pi}{L}\tilde{p} & for \; periodic \; boundary \\ \frac{2\pi}{L}(\tilde{p}+\frac{1}{2}) & for \; antiperidoc \; boundary \end{cases} \tag{4.3.5}$$

$$\tilde{p} = 0,1,2,...,L-1 \tag{4.3.6}$$

Therefore we have to modify the momenta in the Fourier transformation to get $S(p)$. The resulting free Propagator is the same as in the periodic case

$$S(p) = \tilde{m} + \frac{1}{a}\sum_{\mu=0}^{4}\gamma_\mu \sin(p_\mu a) \tag{4.3.7}$$

$$\tilde{m} = m + \frac{1}{a}\sum_{mu=0}^{4}(1-\cos(p_\mu a)) \tag{4.3.8}$$

4.4 Calculating the A and B function

We calculate the propagator in Landau gauge. Therefore we know that it looks like [35]

$$S(p) = \frac{1}{-A(p^2)i\not{p} + B(p^2)} \tag{4.4.1}$$

Our goal is to calculate the A and B function from our lattice calculations. In these calculations, we inverted the Dirac operator $\tilde{D}(p)$ which becomes the continuum Dirac operator for $a \to 0$. The lattice propagator $\tilde{D}^{-1}(p) = \tilde{S}(p)$ has the same property

$$\lim_{a \to 0} \tilde{S}(p) = S \tag{4.4.2}$$

which can be written as

$$||\tilde{S}(p) - S(p)|| \leq \epsilon_a \tag{4.4.3}$$

If a becomes small enough, we can neglect the epsilon on the right hand and we get

$$\tilde{S} = S \tag{4.4.4}$$

We also know that S has a tensor structure which allows us to determine the A and B function from a given S by using $tr(S)$ and $tr(\gamma_\mu S)$. If we combine these two facts we can always get two equations for A and B, if $p \neq 0$. In the following part we use the fact, that $p = (p, 0, 0, 0)$. Therefore only $tr(S)$ and $tr(\gamma_1 S)$ contribute.
We set

$$tr(\tilde{S}(p)) = \tilde{B}(p) \qquad tr(\gamma_1 \tilde{S}(p)) = i\tilde{A}(p) \tag{4.4.5}$$

and calculate that

$$tr(S(p)) = \frac{1}{A} \frac{\frac{B}{A}}{p^2 + \frac{B^2}{A^2}} \qquad tr(\gamma_1 S(p)) = \frac{1}{A} \frac{ip}{p^2 + \frac{B^2}{A^2}} \tag{4.4.6}$$

Now we make use of $S = \tilde{S}$ and after some formula manipulation we get

$$\tilde{A}p^2A^2 + \tilde{A}B^2 = pA \qquad \tilde{B}p^2A^2 + \tilde{B}B^2 = B \tag{4.4.7}$$

We get for $B \neq 0$

$$B = \frac{\tilde{B}p^2}{\tilde{A}^2p^2 + \tilde{B}^2p^2} \tag{4.4.8}$$

$$A = \frac{\tilde{A}p}{\tilde{A}^2p^2 + \tilde{B}^2p^2} \tag{4.4.9}$$

At this point we include the M function

$$M\left(p^2\right) = \frac{B\left(p^2\right)}{A\left(p^2\right)} \tag{4.4.10}$$

$$M = \frac{\tilde{B}p}{\tilde{A}} \tag{4.4.11}$$

To check our results we use the Dirac operator for Wilson fermions (3.5.10) without color($U_\mu = 1$)

$$\tilde{D}(p) = \tilde{m}1 - \frac{i}{a} \sum_{\mu=1}^{4} \gamma_\mu \sin(p_\mu a) \qquad \tilde{m} = m1 + 1\frac{1}{a} \sum_{\mu=1}^{4} (1 - \cos(p_\mu a)) \tag{4.4.12}$$

The inverse

$$S(p) = \frac{\tilde{m}1 + i\frac{1}{a}\sum_{\mu=0}^{4}\gamma_\mu \sin(p_\mu a)}{\tilde{m}^2 + \frac{1}{a^2}\sum_{\mu=0}^{4}\sin(p_\mu a)^2} \tag{4.4.13}$$

delivers

$$\tilde{A} = \frac{\frac{1}{a}\sum_{\mu=0}^{4}\sin(p_\mu a)}{\tilde{m}^2 + \frac{1}{a^2}\sum_{\mu=0}^{4}\sin(p_\mu a)^2} \tag{4.4.14}$$

$$\tilde{B} = \frac{\tilde{m}}{\tilde{m}^2 + \frac{1}{a^2}\sum_{\mu=0}^{4}\sin(p_\mu a)^2} \tag{4.4.15}$$

$$\tag{4.4.16}$$

Rewriting (4.3.8) and (4.3.9) as

$$A = \frac{1}{\tilde{A}}\frac{p}{p^2 + \frac{\tilde{B}^2}{\tilde{A}^2}p^2} \tag{4.4.17}$$

$$B = \frac{\tilde{B}}{\tilde{A}}p\frac{1}{\tilde{A}}\frac{p}{p^2 + \frac{\tilde{B}^2}{\tilde{A}^2}p^2} \tag{4.4.18}$$

and performing the continuum limit $a \to 0$, A becomes 1 and B becomes m. This is the correct results because there is no color. Therefore the propagator is the tree-level propagator

$$S(p) = \frac{1}{-i\not{p} + m} \tag{4.4.19}$$

4.5 Lattice corrections

Combining (4.3.14) and (4.3.15) with (4.3.8) and (4.3.9) we get the lattice results

$$A = \frac{\frac{1}{a}\sin(pa)}{p} \tag{4.5.1}$$

$$B = m + 1 - \cos(pa) \tag{4.5.2}$$

where we used $p = (p, 0, 0, 0)$. For free fermions A should be one and B should be m. Therefore we have to correct the lattice results for A and B to get the corrected results A' and B'. Using multiplicative corrections, we see that

$$A' = A * \frac{ap}{\sin(pa)} \tag{4.5.3}$$

$$B' = B * \frac{m}{m + 1 - \cos(pa)} \tag{4.5.4}$$

delivers the right results for the free fermions. These corrections will also be made for fermions coupled to the gauge fields.

4.6 Renormalization and lattice spacing equal one

The final step to get our results is the renormalization. We use the scheme

$$S(p) = \frac{1}{Z_A A(p)} \frac{i\not{p} + Z_M M(p)}{p^2 + Z_M^2 M(p)^2} \tag{4.6.1}$$

To get Z_A and Z_M we expect that

$$S(p = \mu) = \frac{i\not{p}}{p^2 + m^2} \tag{4.6.2}$$

with the tree-level mass m and the renormalization point μ. Because of the tensor structure, we have two independent conditions which results in

$$Z_A = \frac{1}{A(\mu)} \tag{4.6.3}$$

$$Z_M = \frac{m}{M(\mu)} \tag{4.6.4}$$

At this point we can now discuss the actual calculation. We set the lattice spacing in the Dirac operator to one. Analytically we can describe this as

$$\tilde{D}\left(n|m\right) = \frac{1}{a}\tilde{D}'\left(n|m\right) \tag{4.6.5}$$

$$\tilde{D}'_{\alpha\beta}\left(n|m\right)_{ab} = -\sum_{\mu=\pm 1}^{\pm 4} \left(1 - \gamma_\mu\right)_{\alpha\beta} \frac{U_\mu\left(n\right)_{ab} \delta_{n+\widehat{\mu},m}}{2} + \left(am + 4\right)\delta_{ab}\delta_{\alpha\beta}\delta_{n,m} \tag{4.6.6}$$

where $'$ denotes operators with $a = 1$. First we perform the replacement $am \to m$ which gives us a dimensionless mass. Therefore we call die quantity later m value. We have to do the same with the propagator which gives us

$$\tilde{S}' = \frac{S}{a} = \frac{1}{-aA\left(p^2\right) i\not{p} + aB\left(p^2\right)} \tag{4.6.7}$$

Since a is a constant value we can use the results which we derived earlier by multiplying it with a new factor giving us new A and B functions. On the other hand we multiply these functions with the renormalization constants. Because of their definition, we have to multiply the old renormalization constants with the inverse of this factor to get the new renormalization constants. For this reason the factor cancels in the final results and we can simply use the old results without implementing the new factor.

5 Quenched SU(2) QCD with adjoint fermions

In section (3.1) we introduced QCD. We will now consider quenched SU(2) QCD with adjoint fermions. To get this theory we have to chose the gauge group SU(2) and the adjoint representation for the matter fields. The term quenched means we do not consider the full theory instead we use an approximation(see section (4.1) or [36]).
We will start this chapter with the setup for the calculation. Afterwards we look at the lattice artifacts. We conclude this chapter with the results for the M and the Schwinger function.

5.1 Setup

The quark propagator in quenched SU(2) with adjoint fermions is not a gauge invariant quantity. For that reason we have to implement a gauge fixing for our gauge of choice, namely the minimal Landau gauge. A given code [41] provides the configurations fulfilling all requirements except the link variables are in the fundamental representation. Therefore we have to convert all of them into the adjoint representation

$$U_{\mu}^{adj}(x)_{ab} = \frac{1}{2} Tr\left(\sigma^a U_{\mu}(x)^{\dagger} \sigma^b U_{\mu}(x)\right) \tag{5.1.1}$$

where $\sigma^a,\ a = 1,2,3$ are the Pauli matrices.
We calculate the quark propagator for Wilson fermions

$$\tilde{S}(p)) = \frac{1}{|\Lambda|} \sum_{n,m\in\Lambda} e^{-ipna} D^{-1}(n|m)\, e^{ipma} \tag{5.1.2}$$

$$D_{\alpha\beta}(n|m)_{ab} = -\sum_{\mu=\pm 1}^{\pm 4} (1-\gamma_{\mu})_{\alpha\beta} \frac{U_{\mu}(n)_{ab}\, \delta_{n+\widehat{\mu},m}}{2} + (m+4)\, \delta_{ab}\delta_{\alpha\beta}\delta_{n,m} \tag{5.1.3}$$

using the convention for m in section (4.6). We use three different lattice size $8^4, 16^4$ and 24^4 for six different masses m/a and four different β values which determine the lattice spacing a.

β	a$[fm]$	m_1	m_2	m_3	m_4	m_5	m_6
2.221	0.20	0.01017	0.1017	0.5086	1.017	2.035	10.17
2.328	0.15	0.0076275	0.076275	0.381375	0.76275	1.5255	7.6275
2.457	0.10	0.005085	0.05085	0.25425	0.5085	1.017	5.085
2.656	0.05	0.0025425	0.025425	0.127125	0.25425	0.5085	2.5425
m/a[GeV]	-	0.01	0.1	0.5	1	2	10

Table 1: Used β, m and mass (m/a) values which were used for the different lattice sizes

The combination $\beta = 2.656$ and lattice size 8^4 was not used due breaking of the center symmetry for these parameters(see section (6.2)).
Because the given configurations for technicolor use anti-periodic boundary condition in time direction and periodic boundary conditions in the space directions we also implement these boundary conditions. The most important implication is that we do not have zero momentum (4.5.6) which stems from these conditions. The used momenta are of the form $p = (p, 0, 0, 0)$ where p_0 is the time

direction. Furthermore we have to convert the lattice momenta to the physical momenta.

$$p_{phys} = \frac{1}{2a} \sin\left(2ap_{lat}\right) \tag{5.1.4}$$

The inversion will be done with the biconjugate gradient method [42] for every configuration. Afterwards we calculate the mean value and the errors using a bootstrap algorithm with the assumption that we have an asymmetrical error distribution. The errors for all quantities which we derive from the propagator results (see chapter 4) will be calculated using error propagation.
Finally our renormalization point is 1.5GeV because we want to use the same renormalization point for every β value and which is sufficiently large.

5.2 Lattice Artifacts

In this section we will cover the different effects which appear because we use a lattice. First of all we use a wide range of different masses to study these artifacts. Like momenta also the masses are inversely proportional connected to the lattice distances. Therefore small masses are linked to large distances. The largest distance in a hypercube is $2Na$ where N is the number of points in a spatial or in the time direction. This value is connected to the lattice volume a^4N^4 and therefore connected to the finite volume of the lattice. On the other hand large masses are connected to small distances and the smallest distance on the lattice is the lattice spacing a. For this reason the smallest masses will provide information about the finite volume artifacts while the largest masses will provide informations about the lattice spacing artifacts. An other effect is a phase transition which depends on β and N. This lattice artifact will not be covered because we already regarded it by excluding the case $\beta = 2.656$ and $N = 8$. This effect will become important in the technicolor section.
All these artifacts influence our result and add systematical errors. Since we have no systematical control over these errors we can only determine lower bounds for the errors.

5.3 Mass dependence

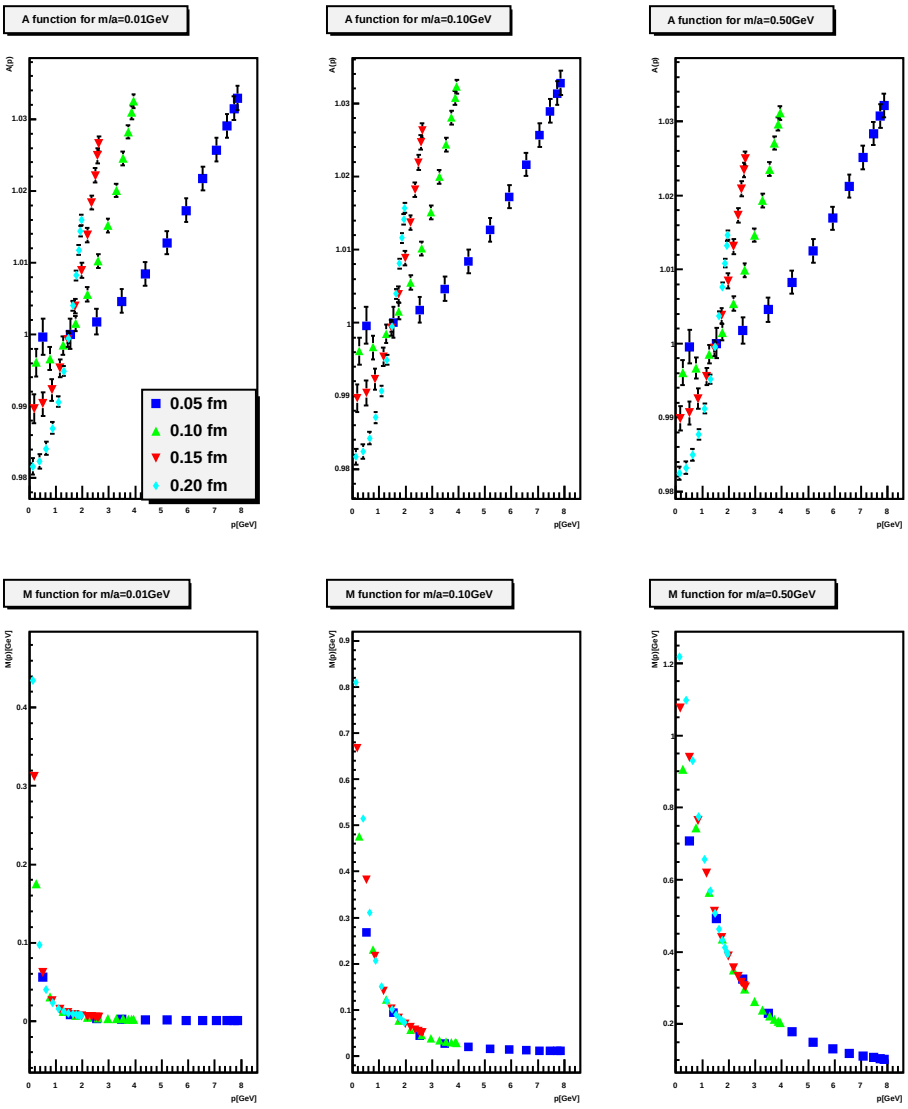

Figure 1: Resulting A and M functions for diferent lattice spacings and a lattice size of 24^4.

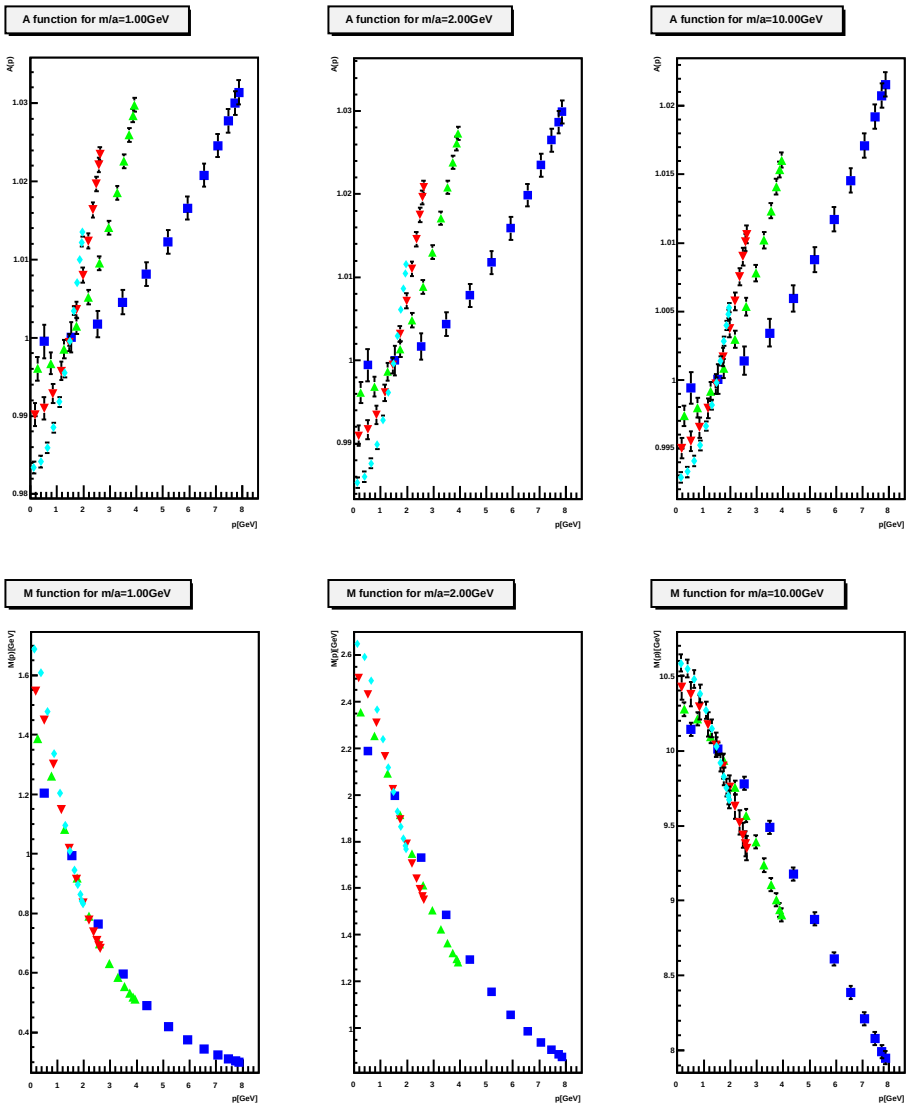

Figure 2: Resulting A and M functions for different lattice spacings and a lattice size of 24^4. The Legend can be found in figure 1.

In the figures 1 and 2 we see the A and M functions for different masses. The prominent feature for all masses is that the A functions never coincide for different lattice spacings. Further investigation shows that the difference between the A functions is a scale factor. On the other hand a test for the free case (link variables equal to one) showed that the A function delivers the right result. Therefore we assume this to be a systematical error. Despite this fact we see that the A function is close to one. The deviation for every momentum values is below 0.04 and therefore below 4% of the value one. For this reason we set the A function equal to one for every momentum value with a relative error of 4%.

We now look at the largest mass 10GeV. In contrast to the other masses we see that the M functions do not coincide for different lattice spacings. As we already discussed this effects stems from the lattice spacing. Albeit we already see this lattice artifact here we can not be sure of the influence of the lattice volume. Therefore we will investigate this artifact later.
Looking at the smallest masses we surprisingly see that the graphs coincide. As these small masses are stronger influenced by finite volume effects we would expect much more derivation between the different graphs. This fact could stem from the different lattice spacings. We will discuss this issue later.
The last prominent feature of the figures are the error bars. While the A function has error bars for every value, the M function has error bars only for the largest mass. This result comes from the error propagation. Carefully calculating these error show that the errors are proportional to the value

$$\Delta A_r = \Delta\left(Z_A A\right) = A_r \left(\left(\frac{\Delta Z_A}{Z_A} \right)^2 + \left(\frac{\Delta A}{A} \right)^2 \right)^{\frac{1}{2}} \tag{5.3.1}$$

$$\Delta M_r = \Delta\left(Z_M M\right) = M_r \left(\left(\frac{\Delta Z_M}{Z_M} \right)^2 + \left(\frac{\Delta M}{M} \right)^2 \right)^{\frac{1}{2}} \tag{5.3.2}$$

Since $A\left(p^2\right)$, $M\left(p^2\right)$,Z_M and Z_A are functions of $\tilde{A}$ and $\tilde{B}$ their errors depend on the errors of these values $\Delta\tilde{A}$ and $\Delta\tilde{B}$. Assuming that those errors are of the same order for different momenta and masses also the order of the error bars will depend only on the order of the actual value. Looking at the A function we see that all values are close to one. Therefore with this assumption all error bars should be of the same same order which we observe. On the other hand for the M function the range of the $M\left(p\right)$ axis changes roughly by a factor of four while the order of the mass changes by a factor of 1000. Therefore the error bars grow roughly by a factor of 250 in the graphs. This explain why we see the error bars only for the biggest mass.

5.4 Finite volume artifact

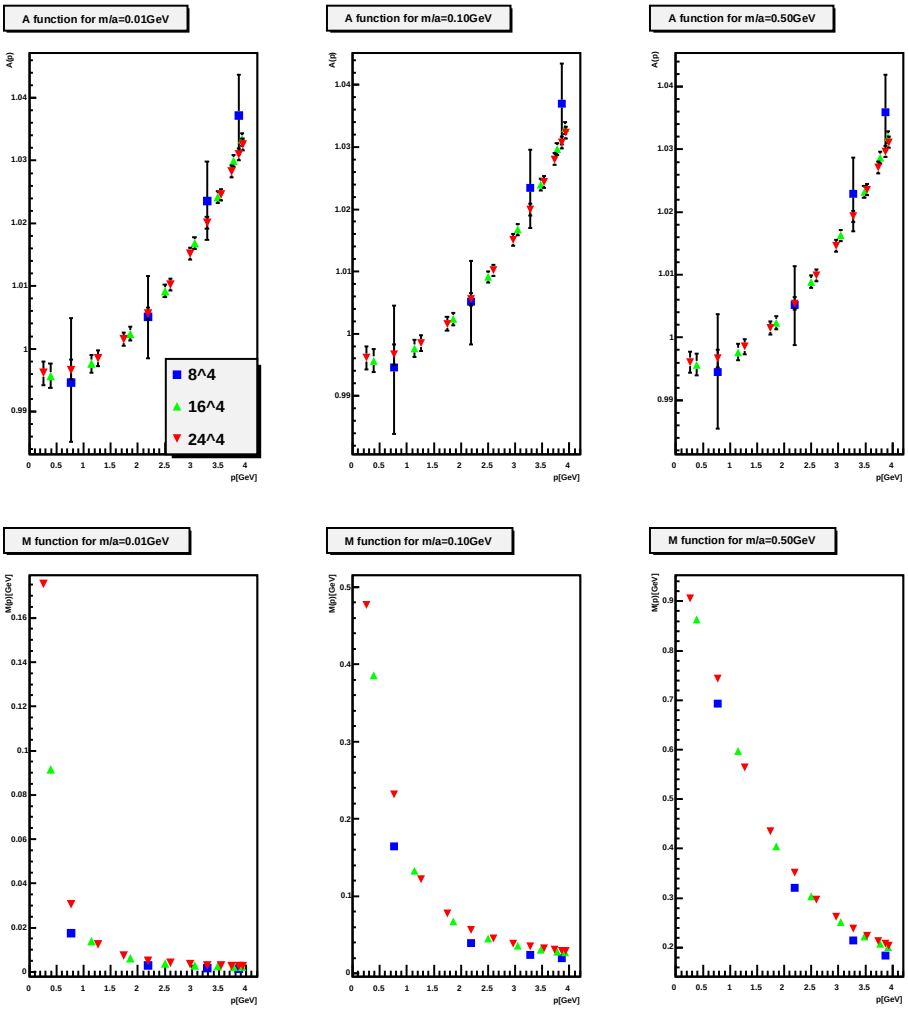

Figure 3: Resulting A and M functions for different lattice sizes and a lattice spacing of 0.1fm.

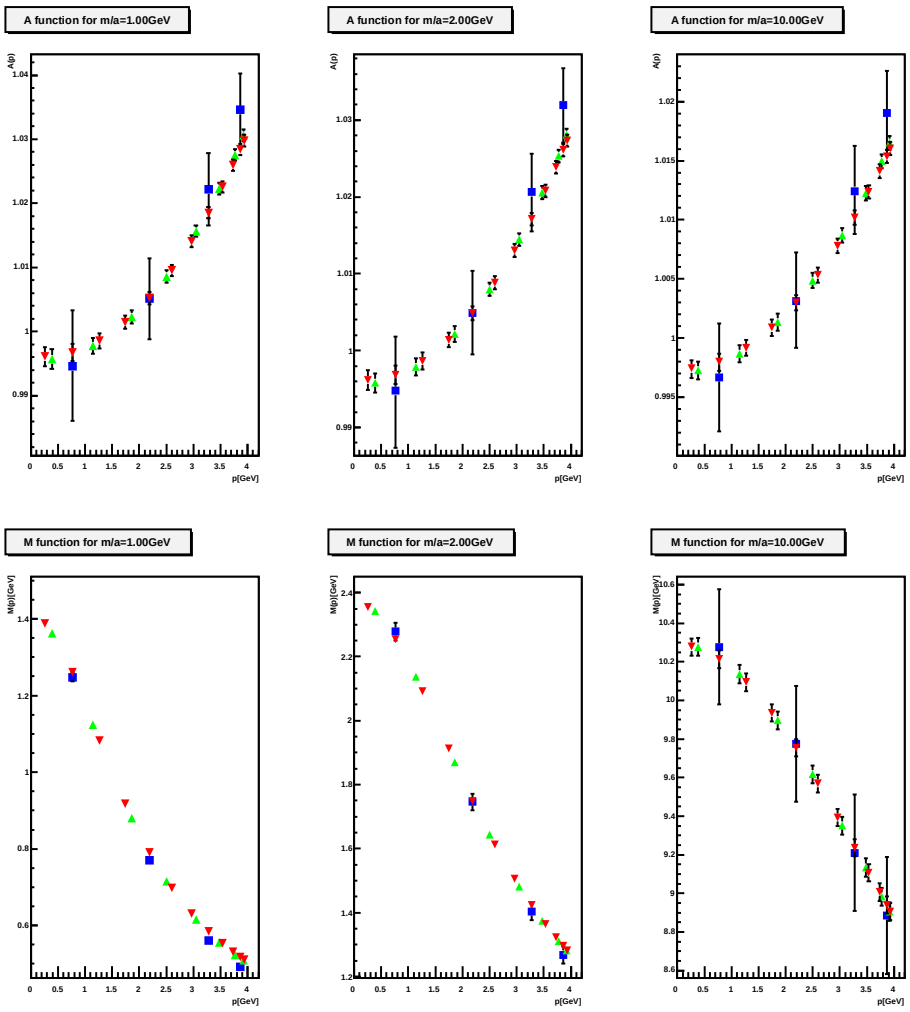

Figure 4: Resulting A and M functions for different lattice sizes and a lattice spacing of 0.1fm. The legend can be found in figure 3.

As we have seen in the last section, the M functions for the smallest masses coincide. Since these masses are most senstive to finite volume effects, these results suggest that we do not have such contributions. However the simultaneously change of the lattice spacing could compensate the finite volume effects. For this reason we have to further investigate this matter. In the figures 3 and 4 we see the graphs for different lattice sizes while the lattice spacing remains always the same. Again we look at first at the A function. We see all graphs coincide for the different masses. Therefore we assume there are no fnite volume effects present in the A function. looking at the M function we see a difference between the largest and the smallest masses. There is no effect present for the three largest masses. For the three smallest masses we see a difference between the different values which increases with smaller mass which shows that the small masses are indeed stronger influenced by finite volume effects. For the smallest mass and the lowest momentum in the 8^4 lattice we get a

70% relative error. This relative error decreases to roughly 10% for the same momentum and the mass 0.5GeV. Since we still see a difference between 16^4 and 24^4 further investigation for larger lattice volumes are necessary to get full systematical control for this error. Anyhow since this error decreases for with larger momenta we assume a 10% relative error for the mass 0.5GeV
Again we see an interesting effect for the error bars. The error bars also depend on the lattice size. This effect comes from the inversion process. Basically we average over the whole lattice while we invert the Dirac operator. For this reason the error decreases for larger lattice sizes. However this process will only decrease the error coming from the statistical distribution of the configurations. For this reason the error will converge to a value which depend on other error sources. This can be observed in the fact that the error bars for the two largest lattices are almost the same.

5.5 Continuum limit

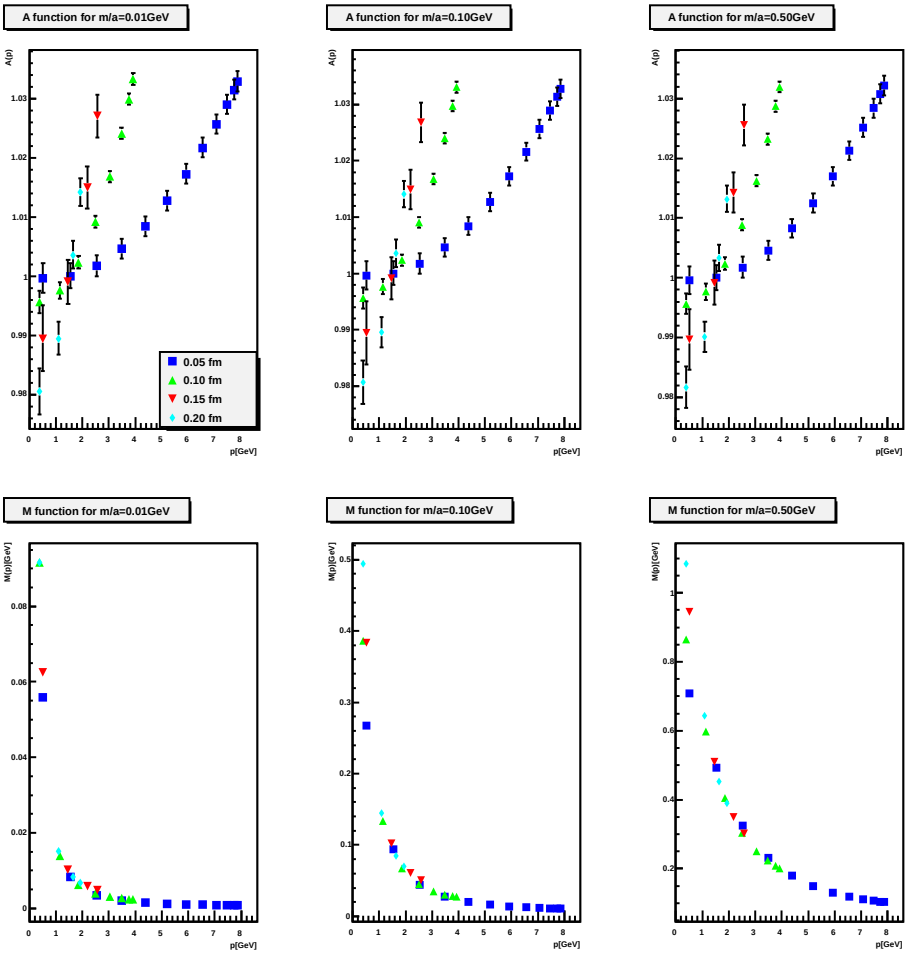

Figure 5: Resulting A and M functions for roughly constant volume $Na = 1.2$fm and $Na = 1.6$fm and different lattice spacings.

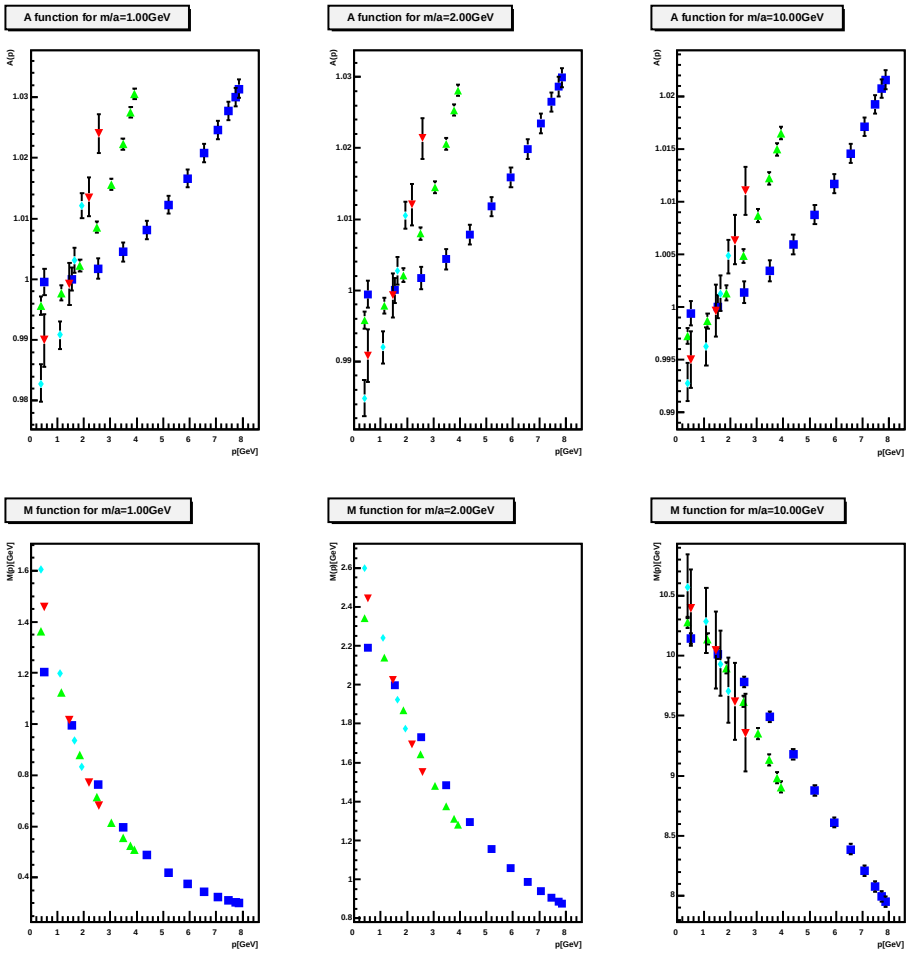

Figure 6: Resulting A and M functions for roughly constant volume $Na = 1.2$fm and $Na = 1.6$fm and different lattice spacings. The legend can be found in figure 5.

In the last section we varied the lattice size while keeping the lattice spacing constant. Now we will vary the lattice spacing while we keep the lattice volume constant. This is actually the continuum limit which is shown in the figures 5 and 6. We see that the values for the lowest momentum differ greatly. Since we did not observe such a behaviour for the mass 1GeV in the section beforehand we infer that this effect comes from the continuum limit. Like the finite volume effect, we encounter a decrease of the relative error for larger masses.
Looking again at the different masses we see there is no big difference between the graphs for the smallest mass while the graphs for the biggest mass do not coincide. This shows that the largest mass is indeed stronger affected by the lattice size. Despite this fact the relative error for the largest mass is around 10%. Therefore this effect is comparable with the finite volume effect. Again further investigation for smaller lattice size is required to have full systematic control for this error.

5.6 Summary

We unexpectedly found that the lattice artifacts do not strongly alter the graphs for the smallest and the biggest masses. Still we found the beforehand mentioned influence of the finite size effect for the smallest masses and the lattice size effects in the largest masses. Despite these effects we have results for masses ranging from 0.01GeV to 10GeV but we have to take care for 10GeV since the error from the lattice spacing became close to 10% for all values. On the other hand we found that the values for momenta below 1 GeV are unreliable for all masses except 10GeV because either they are strongly influenced by the finite size effects or are strongly influenced by the continuum limit. Here we want to emphasize that all these discussions can only give a lower bound to the errors.

5.7 Results

As we have already seen the A function has a systematically error. Therefore the only reliable result for this function is that it is close to one for the whole momentum range. For this reason we will discuss only the mass function and the Schwinger function. As we have already seen the

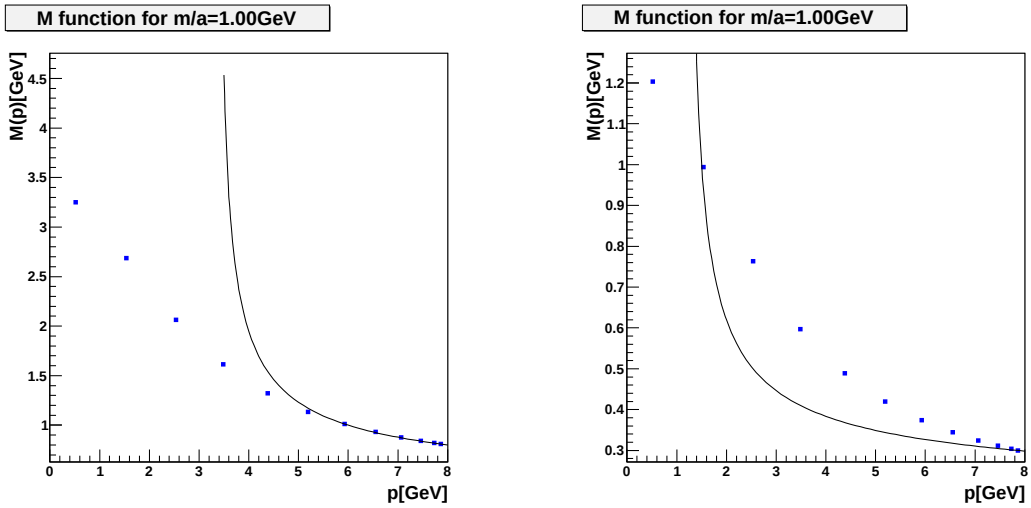

Figure 7: M functions for two different renormalization points with a fit for the perturbative result. Left is the renormalization point 6GeV and right is the renormalization point 1.5GeV.

A function has a systematically error. Therefore the only reliable result for this function is that it is close to one for the whole momentum range. For this reason we will discuss only the mass function. The figures 5 and 6 show the results for an almost constant volume. Here we also see that the value for the lowest momentum is not dominated by a finite volume effect because the volume is almost constant for all graphs. Since we also saw this behaviour for the same lattice spacing and different lattice sizes it seems this effect is a combination of the limit $a \to 0$ and finite volume effects. Investigating the continuum limit further we see that the graphs coincide for $p > 1$GeV and the masses smaller than 10GeV . On the other hand we have to add at least 10% systematical error for 0.5GeV and even more for smaller masses coming from the finite volume effects. Within a

10% relative error also the graphs for m=10GeV coincide. Therefore we regard only the mass 1GeV in the following because it was neither strongly influenced by the finite volume effects nor by the lattice spacing effects. Therefore those results seem to be good continuum estimations.
Looking at the infrared we see an increase in the mass functions. This infrared enhancement was already observed for adjoint fermions in SU(3) in continuous space[43]. For large momenta the function should show the asymptotic behaviour we know from perturbation theory [34]. To check this we have to first introduce the perturbative result.

$$M\left(p^2\right) = M\left(\mu\right)\left(\omega \log\left(\frac{p^2}{\mu^2}\right) + 1\right)^{-\gamma} \tag{5.7.1}$$

$$\gamma = \frac{12}{11N_c - 1N_f} \tag{5.7.2}$$

$$\omega = \frac{\beta_0 \alpha\left(\mu\right)}{4\pi} \tag{5.7.3}$$

$$\beta_0 = \left(\frac{11N_c}{3} - \frac{2N_f}{3}\right) \tag{5.7.4}$$

where $\alpha\left(\mu\right)$ is the running coupling and μ is the renormalization point. Since we can not determine this quantity directly we use it as a fit parameter for our curve. The quantities N_c and N_f are the number of colors and the number of flavors. In SU(2) we have 2 colors. The number of flavors is for the quenched zero. The results for the fit can be seen in figure 10. Looking at these results for the mass 1GeV we see that the fit only matches our result for the last three momentum points. To get a better fit to the perturbative results, we increased our renormalization point to 6GeV. We see this fit in figure 7 on the right hand side. We conclude from this fact, that the used perturbative result is not accurate for the region around 1.5 GeV. For this reason we need perturbative results for higher orders to access the quark propagator for smaller momenta than 5GeV which we see in the figure. Of course we can not get the full propagator with the perturbation theory because we have non perturbative effects.

5.8 Schwinger function

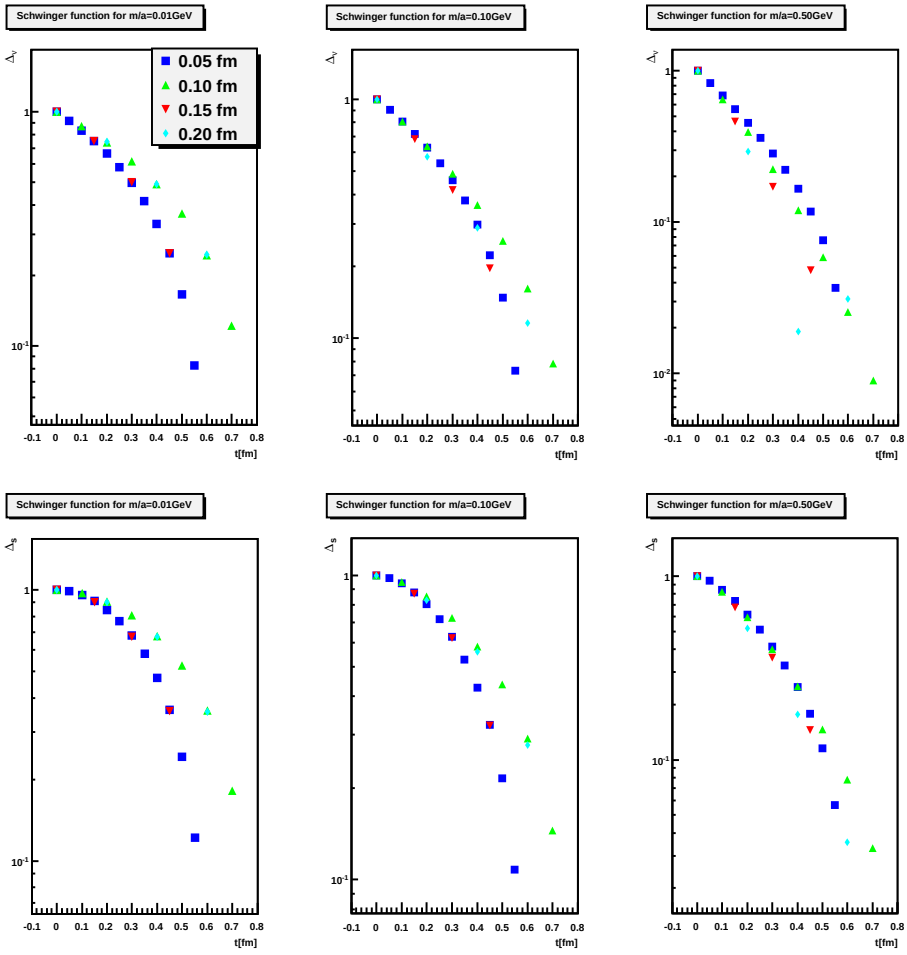

Figure 8: Schwinger functions for roughly constant volume $Na = 1.2$fm and $Na = 1.6$fm

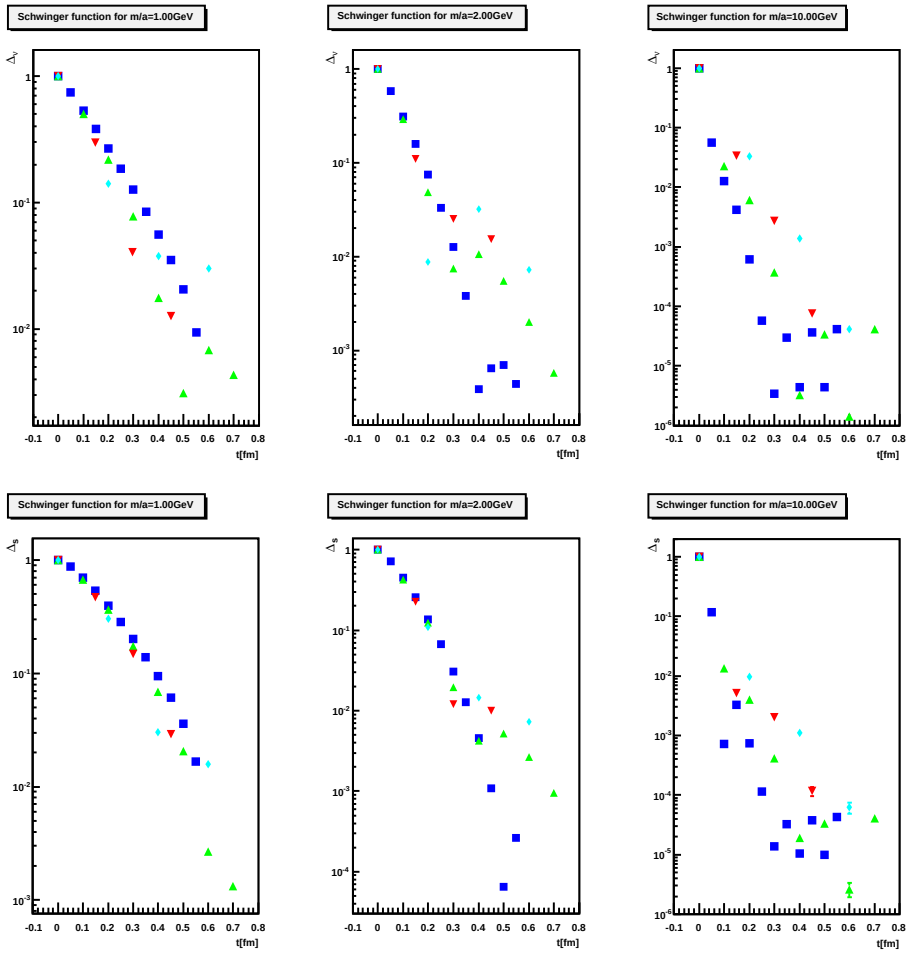

Figure 9: Schwinger functions for roughly constant volume $Na = 1.2$fm and $Na = 1.6$fm. The legend can be found in figure 8.

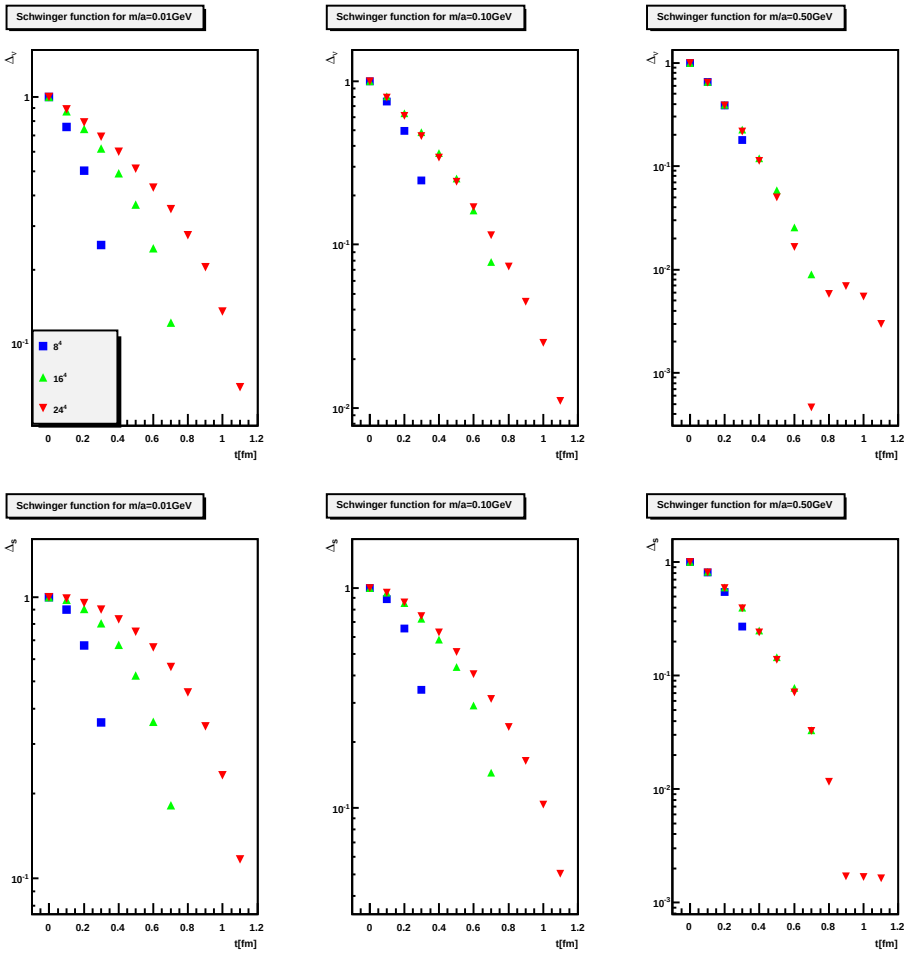

Figure 10: Schwinger functions for different volumes but constant lattice spacing 0.1fm.

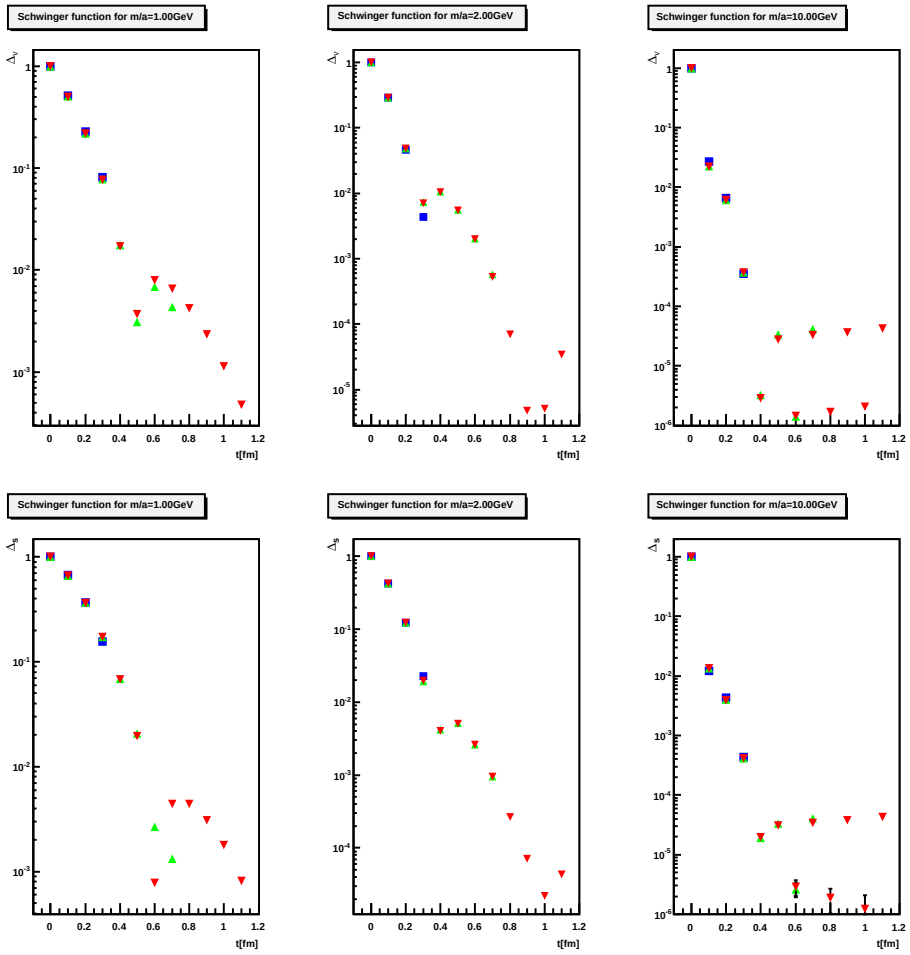

Figure 11: Schwinger functions for different volumes but constant lattice spacing 0.1fm. The legend can be found in figure 10.

The results for the Schwinger functions are given in the figures 8-11. Since we have two different possible Schwinger functions coming from (4.2.6) and (4.2.7), we will denote them by Δ_ν and Δ_s. We clearly see a positivity violation for both functions. This implicates that the adjoint quarks in quenched SU(2) are unphysical particles.
Looking at crossing point we find that it is shifted to smaller values for larger bare masses. This effect is plausible because a larger mass is connected to smaller distances in position space. Another interesting effect shows up in the figures 11-16. While the zero crossing always at the same time value for the constant lattice spacing case it shifts in the continuum case. In this plot also the volume varies between $1.2fm$ and $1.6fm$ but nonetheless we see also a shift between the graphs for the same lattice size. Therefore the zero crossing point depends on the lattice spacing. As we can not say for sure if this is a real shift or just an increase for the values we need again further investigation for smaller lattice spacings.

6 Minimal Walking Technicolor

In this chapter we will calculate the quark propagator for the minimal walking technicolor theory, introduced in chapter two. Afterwards we derive the anomalous mass dimension from our result. Other results shown that this quantity should be small compared to one [9][10][11][12][6][7][13]. Furthermore we will also calculate the Schwinger function.

6.1 Setup

The setup for the calculation is almost the same as the setup of the quenched SU(2) QCD case. The configurations were provided by the authors of the paper [6] with methods described in this paper. There are already results which use these configurations. These results include the 0^{++} and 2^{++} glueball, the pseudoscalar and vector meson mass, the PCAC masses and the string tension [6][7]. All these results suggest that we reach the chiral limes for $m = -1.2$.
Apart from the configurations, we will use an asymmetric lattice of the form $N_t \times N_s^3$ and we get new masses(see table 2). It is apparent in the table that the lattice spacing is dependent on the m value. The reason for this feature is the scale setting process. We demanded that the technigluebal mass is $2TeV$ for every configuration. Since this value is dependent on the technigluon mass, which in turn is dependent on the value m, we get that the lattice spacing is dependent on the value m. A more detailed analysis of the scale setting can be found in [44]. We have chosen the renormalization point $\mu = 4TeV$
Apart from these changes we use the same algorithms and techniques which we already used for quenched SU(2) QCD in chapter 5.

6.2 Phase transition

In this thesis we consider only SU(2) gauge theories with fermions in the adjoint presentation. The associated action has a $\mathbb{Z}_2$ symmetry. This symmetry is the center symmetry which we find for infinite volume. Since we only consider finite volumes it is possible that this symmetry is spontaneously broken. For this reason we have two distinct phases, one with broken center symmetry and one with unbroken center symmetry. We have also these two phases for the used technicolor configurations[6][7]. The results show that we have unbroken center symmetry for the 16×8^4 lattice above $m = -0.975$. The same is true for the 24×12^3 lattice above $m = -1.05$. There is no configuration for the 32×16^3 lattices with definitive unbroken center symmetry. We consider for our results only configurations with unbroken center symmetry but the results for the other phase can still provide interesting effects. For this reason we did the calculation for all configurations.

$-m_0$	β	a^{-1}[TeV]	N_t	N_s	configurations
-0.500	2.25	1.66	16	8	720
-0.250	2.25	1.73	16	8	720
0.000	2.25	1.76	16	8	720
0.250	2.25	1.81	16	8	720
0.500	2.25	1.91	16	8	720
0.750	2.25	2.18	16	8	720
0.900	2.25	2.22	16	8	720
0.950	2.25	2.52	16	8	720
0.975	2.25	2.74	16	8	720
1.000	2.25	3.04	16	8	720
1.025	2.25	3.42	16	8	719
1.050	2.25	3.92	16	8	719
1.075	2.25	4.59	16	8	1171
1.100	2.25	5.51	16	8	1035
1.125	2.25	6.79	16	8	918
1.150	2.25	8.63	16	8	882
1.175	2.25	11.3	16	8	763
1.200	2.25	15.4	16	8	689
0.950	2.25	2.52	24	12	948
1.000	2.25	3.04	24	12	809
1.050	2.25	3.92	24	12	153
1.075	2.25	4.59	24	12	152
1.100	2.25	5.51	24	12	154
1.125	2.25	6.79	24	12	157
1.150	2.25	8.63	24	12	147
1.175	2.25	11.3	24	12	256
1.180	2.25	12.0	24	12	419
1.185	2.25	12.8	24	12	403
1.190	2.25	13.6	24	12	381
1.200	2.25	15.4	24	12	255
1.175	2.25	11.3	24	24	8
1.150	2.25	8.63	32	16	320
1.175	2.25	11.3	32	16	181
1.180	2.25	12.0	32	16	227
1.190	2.25	13.6	32	16	21
1.200	2.25	15.4	32	16	60

Table 2: The β, m and a values for the different lattice configurations. The column configurations list the actual used configurations. We also had configurations for the lattice sizes 64×16^3 and 64×24^3 but the calculation time became to large for these configurations. For this reason we did not calculated the quark propagator for these configurations.

6.3 $\tilde{A}$ and $\tilde{B}$ function

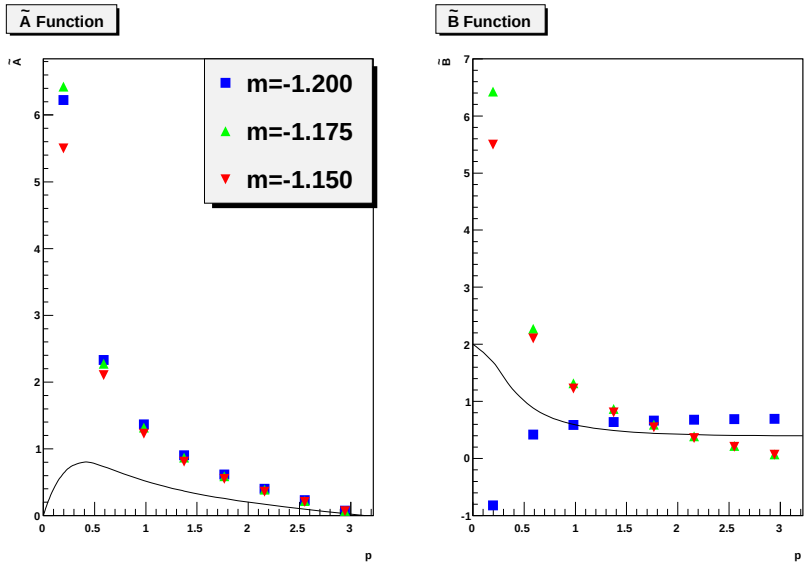

Figure 12: $\tilde{A}$ and $\tilde{B}$ function for $m = -1.150$,$m = -1.175$ and $m = -1.200$ for the lattice size 16×8^3. The solid line is the result for the free fermion case.

In this section we will discuss the $\tilde{A}$ and $\tilde{B}$ function which were introduced in section (4.3). The reason for the interest in the functions comes from an unexpected behaviour which we did not saw for quenched SU(2) QCD. In figure 12 we see the graphs for three different m values which are close to the chiral limes. In contrast to the graph for $m = -1.150$ the two other graphs increase with increasing lattice momentum p. For $m = -1.2$ there is even a zero crossing. This results also in a zero crossing for the M function because the $\tilde{A}$ function has no zero crossing in the same lattice momentum range. However as these results are for the 16×8^3 lattice, this problem will not influence our results because the spurious phase transition is at $m = -0.95$.
Looking at even bigger lattices we find the same behaviour. For 24×16^3 and 32×24^3 lattice sizes, the $\tilde{B} function$ becomes negative for $m = -1.150$. We see that this effect affects bigger masses for larger lattice sizes while the spurious phase affects smaller masses for larger lattices. This means this effect could influence the results for the larger lattices.
A possible explanation is that this effect comes from the additional mass term which we get for Wilson fermions. To investigate this matter we took the configurations for the 16×8^3 lattice with $m = -1.2$ and increased the m value in the Dirac operator. In figure 13 we see the results. We already observe for $m = -1.1$ that the $\tilde{B}$ function is always positive and stays positive for even larger masses. Furthermore looking only at the lowest momentum for different m values we observe a maximum between $m = -1.1$ and $m = -0.9$. For $m = -0.9$ the $\tilde{B}$ function seems to become like the $\tilde{B}$ function for the free fermion case. For even larger masses the results transforms even further but it seems the $\tilde{B}$ trend to a specific function. Anyhow, the results of this investigations show that the observed effect is indeed dependent on the m value. Therefore it is possible that this effect is a lattice artifact which stems from the additional Wilson term which modifies the mass.

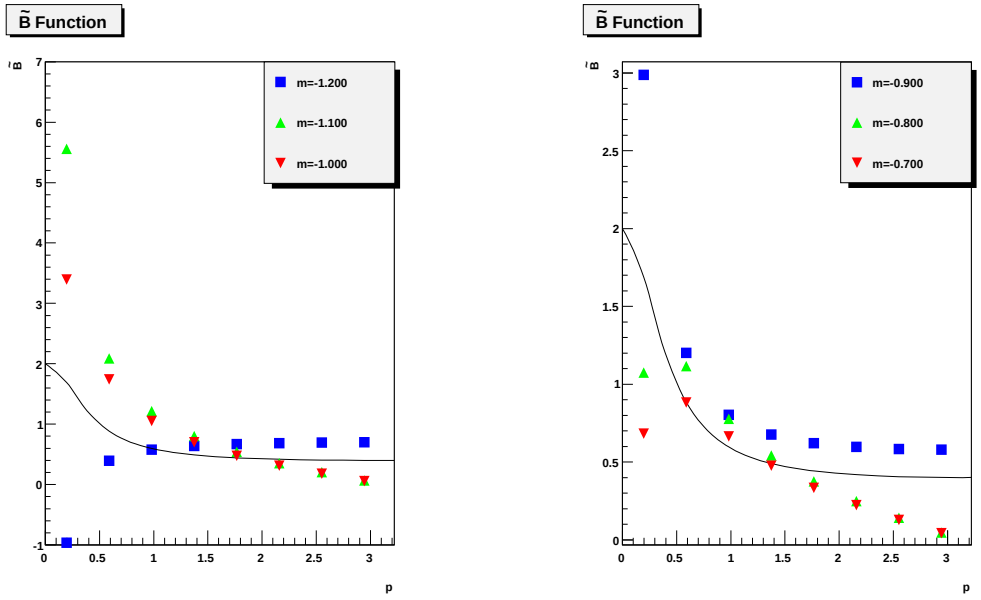

Figure 13: $\tilde{A}$ and $\tilde{B}$ function for different m values in the Dirac propagator and lattice size 16×8^3. The solid line is the result for the free fermion case.

6.4 Asymmetry lattice artifacts

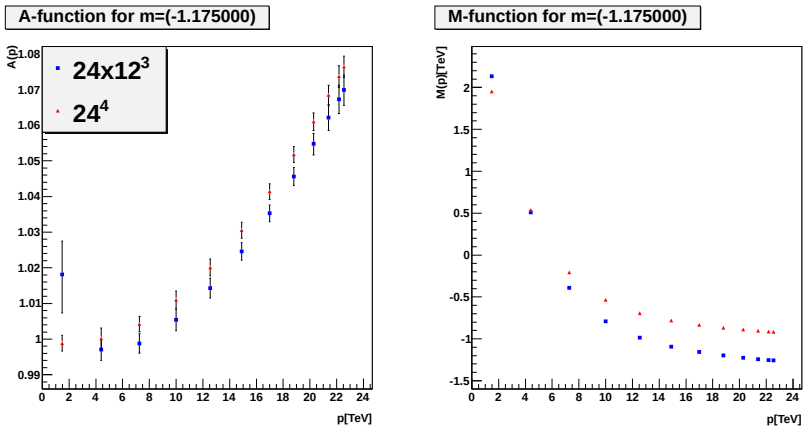

Figure 14: A and M function for the 24^4 and 24×12^3 lattices with the mass $m = -1.175$

Because we use asymmetric lattices, we expect that our results will differ from symmetric lattices. This effect is shown in figure 14. Looking first at the A function we see that all values are shifted by roughly 1% relative error. Furthermore we see that the possible interesting effect for the lowest momentum in the A value seems to be just a lattice artifact which should vanish for symmetric lattices. On the other hand we see that for the M function the values for the lowest momenta coin-

cide. The difference between both graphs increases for larger momenta and seems to be momentum dependent. The relative error assumes roughly 100% for the third smallest momentum value and decreases afterwards to roughly 50% for the largest momentum. Therefore we have large lattice artifacts for the M function. On the other hand the M function has a zero crossing. This means we have already the lattice artifact which we discussed beforehand. Since we can not determine the outcome if we combine both lattice artifacts the results for the M function, we assume that the results for the errors presented here are unreliable for the M function. Therefore we can only assume the error for this artifact for the M function.

6.5 Finite volume artifacts

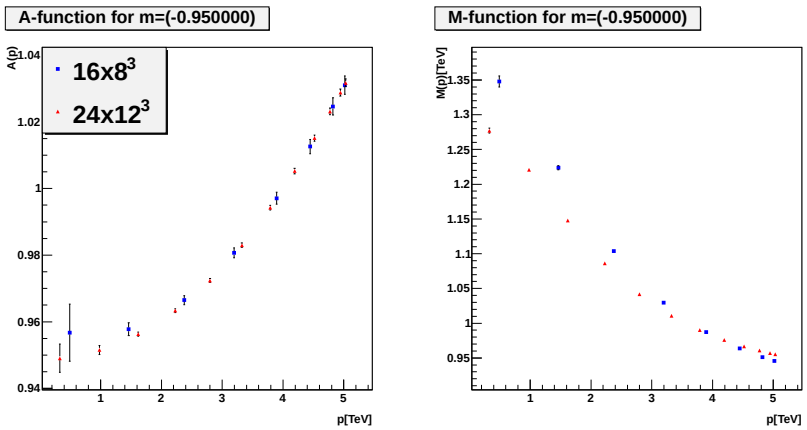

Figure 15: A and M function for same lattice spacings and different volume. Displayed are the results for the configurations 16×8^3 and 24×12^3 for the mass $m = -0.95$.

In figure 15 we see two different graphs for different lattice volumes. Looking first at the A function we see that both graphs coincide. We also see once again that the error bars shrink with larger lattice sizes. On the other hand we see that the graphs for the M function differ. This results hints that there are indeed finite volume artifacts. However we should not forget that we also have the already examined fact, that there is also the effect described in section 1.3. As this effect also scales with the lattice size we expect that it also influence both graphs with different effects. For this reason we can not be sure if the observed differences are only finite volume effects. However we observe a relative error of roughly 6% for the lowest momentum which decreases with increasing momentum.

6.6 Border of the phase transition

In figure 16 we see the M function for two different techniquark masses. One mass is just below the phase transition and the second one is at the border of the phase transition. We see a large difference in the behaviour of both functions as one graph is constantly decreasing with increasing momenta while the other is increasing at the same time. As this effects occur on the border of the two phases it is possible that this effects comes from the phase transition. For the smaller lattice 16×8^3 we experience the same effect but not on the border of the two phases. Instead we see the

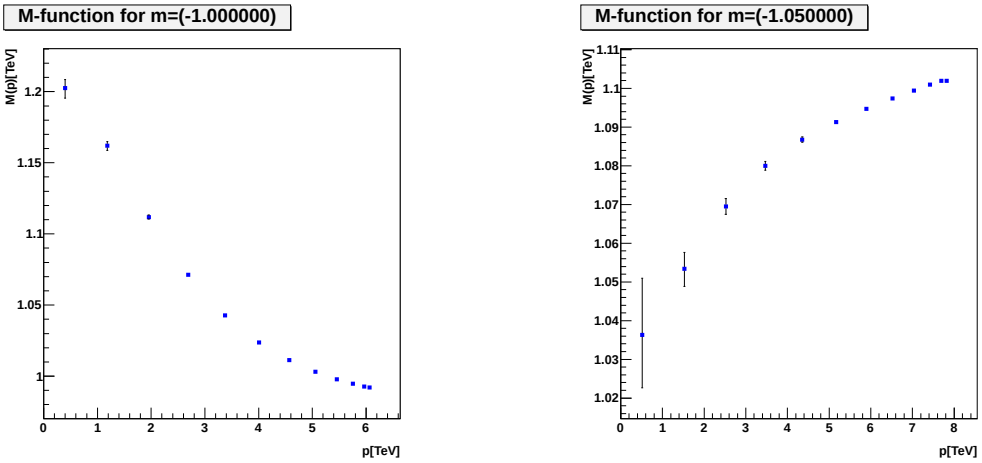

Figure 16: M function for the lattice size 24×12^3 with $m = -1.00$(left) and $m = -1.05$(right).

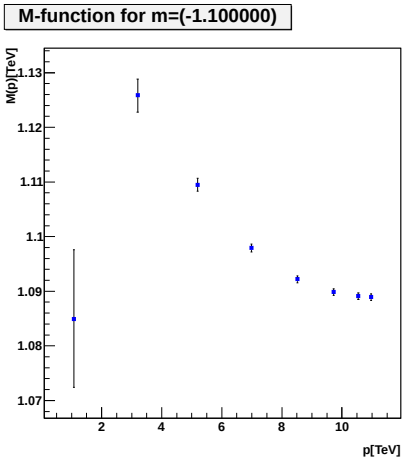

Figure 17: M function for the lattice size 16×8^3 with $m = -1.10$

transition from one graph to the other at $m = -1.10$ shown in figure 17. Here we see that the lowest momentum value is already lower than the value for the second lowest momentum value. For the lattices size 32×16^3 we observe this effect for any lattice. As the biggest mass available lies on the border of both phases we can not say anything about this effect for this lattice size. Since we experienced this effect only in the wrong phase, it should not effect our results. However as this effect goes to higher mass values for bigger lattice sizes it could influence results which use larger lattices. On the other hand it could be that this effects indicates a wrong phase. Still we need further investigation into this matter before we can make a clear statement.

6.7 Summary

We found two interesting effects in the phase with broken center symmetries. Since we have no configuration for the lattice size 32×24^3 with unbroken center symmetry, we could no determine if these effects are also present in the correct phase. For this reason we can not say to which extend these effects influence our results. Furthermore we looked at the asymmetric lattice artifact. We saw a zero crossing for the M function which shows that the result is influenced by at least one effect mentioned beforehand. For this reason the found error is a combination of different effects. For this reason it is unreliable. The same could be true for the finite volume size artifact. Here we are not sure if the influence is present because we did not saw a zero crossing but the second effects also scales with the lattice size.
Summing up all these results we see that further investigations for the artifacts in section 1.3 and section 1.6 is needed before we can examine the remaining lattice artifacts. Since these artifact only show up in the wrong phase, we assume that these artifacts are connected to the wrong phase. On the other hand we assume that the finite lattice volume effects and the asymmetry effects are not too severe. With this assumption in mind, we will calculate the quark propagator for the configurations with unbroken center symmetry.

6.8 Results

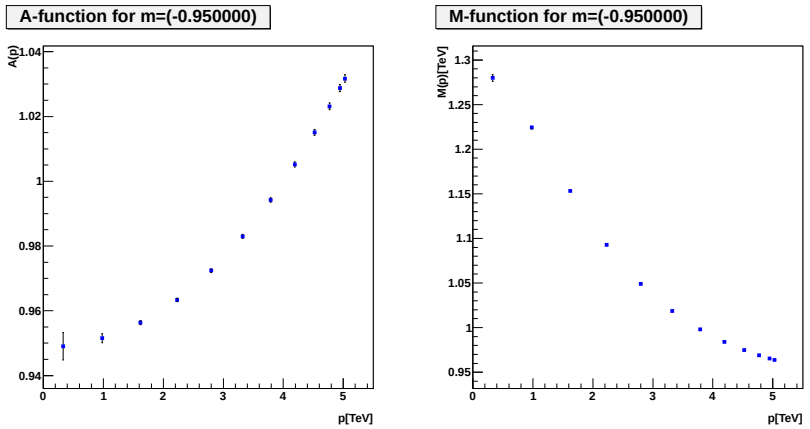

Figure 18: A and M function for the lattice 24×12^3 with the mass $m = -0.95$.

First we look at the A function in figure 18. Since we did not change anything in the algorithm to determine the A function, we once again assume we have the same systematical error which we had for quenched SU(2) QCD. For this reason we assume the A function is one for the whole region with a relative error of less than 4%.
Looking at the M function we observe again the same behaviour as we have seen in the quenched SU(2) QCD case which means we have an infrared increased value while it decreases with larger momenta. The main task is now to extract the anomalous dimension. For this we fit the result to the function

$$\frac{1}{a}\left(\omega \log\left(x\right) + k\right)^{-\gamma} \tag{6.8.1}$$

where a, ω and γ are fit values. It is possible to get back the asymptotic form in section (5.7) by some formula manipulation. We identify γ as the anomalous mass dimension. We used for all fits momentum values above 2TeV because it improved the fit for the large momenta. Again we want to emphasize the different phases which reduces the usable configurations to only three for which we know the PCAC mass. To get an additional result we linear extrapolated the PCAC mass to $m = -0.9$. Any further extrapolation for the PCAC masses seemed to be unreliable because the value for am_{PCAC} began to decrease for $m = -0.75$ which is a behaviour we never observed for this value. For this reason we discarded this configuration. The results can be seen in table 3. We did not gave any errors because they were all below 1% relative error. On a side note: Using the fit parameters to get back the asymptotic form from section (5.7) while setting $M(\mu) = m_{PCAC}$ we get that $\mu \sim 4$. This shows that the used perturbative result is reliable for the momenta above 2 TeV.
We see that the γ value is small compared to one which is in accordance with previous results [9][10][11][12][6][7][13]. We further see that the anomalous mass dimension decreases if we come close to the chiral limit. For this reason we assume that it will be even smaller in the chiral limit which we suspect to be at roughly $m = -1.2$. Looking at the results for different lattice sizes we see a difference in the γ value for the same m value. This means we have a finite volume effect. For this reason further investigation is needed to get rid of this effect.

6.9 Schwinger function

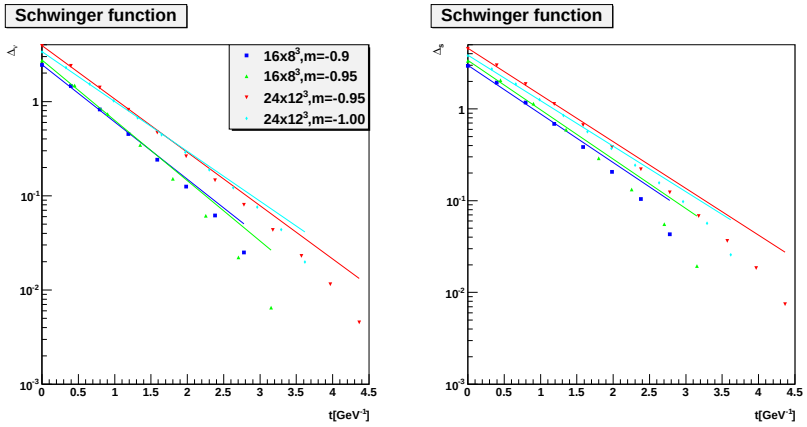

Figure 19: Schwinger functions for the lattice 16×8^3 with the mass $m = -0.95$.

We also looked at the Schwinger functions which are displayed in figure 19. In contrast to quenched SU(2) QCD we see no zero crossing for all considered configurations. For this reason we can not state if techniquarks are physical or unphysical particles. However we can determine the mass because we have a real pole. Therefore the Schwinger function is proportional to $e^{-m_{est}t}$ with m_est the mass of the techniquarks[40]. Because we have two different Schwinger functions we get to estimated masses which are displayed in table 2. Again, the calculated errors were below 1% relative error. We see that theses masses decreases if we come closer to the mass $m = -1.2$ which is expected since we expect massless fermions in the chiral limit. However we observe again a finite volume effect in the masses.

$N_t \times N_s^3$	m	γ	ω	k	m_{est}[TeV] from Δ_ν	m_{est}[TeV] from Δ_s
16×8^3	-0.90	0.50	2.41	2.12	1.47	1.24
16×8^3	-0.95	0.33	10.29	3.57	1.40	1.22
24×16^3	-0.95	0.23	31.32	10.21	1.30	1.17
24×16^3	-1.00	0.10	31.17	10.33	1.22	1.14

Table 3: Results for the anomalous mass dimension, the fit values and m_est

7 Conclusion and Outlook

We have calculated the two point function for quenched SU(2) QCD and MWT. In the first case we found that the A functions for different lattice sizes did not coincide. We assume that this is a systematical error. For this reason our result is that the A function is one with a relative error of 4% for the whole momentum region which we consider. On the other hand we did not found such a behaviour for the M function. Looking at large momenta our results were in agreement with the perturbation theory. Here we note that the perturbative result was in accordance with our results only for momenta around and larger than 5GeV. Looking at the infrared region we found an enhancement which is in agreement with a result for SU(3) QCD[43]. Both facts show that our results should be reliable. With these results we were able to calculate the Schwinger function which turned out to have a zero crossing which shows that a single quark is an unphysical particle. As we found that the zero crossing changes if we look at the continuum limit further investigation is necessary. For this reason, the next step for quenched SU(2) is to perform the calculations for a 64^4 lattice which enables us to combine the lattice sizes and lattice spacings in such a way that we have always the same volume $0.32^4 fm^4$. Expecting that we still see the shift of the zero crossing in this case it would be interesting to look at other lattice spacing and lattice size combinations. However to achieve these next steps we have to modify our calculation algorithm because the calculation time was too long to get the results for the 64^4 lattice. Therefore the actual next step would be to improve our algorithm before calculating the larger lattices.
We did the same for MWT which we did for the quenched SU(2) QCD. Here we found the same behaviour for the A function. For this reason we assume that there is also a systematical error present. For this reason we also have the result that the A function is one with a relative error of 4%. Furthermore we found an interesting behaviour for our results in the center symmetry broken phase(see section (6.3) and (6.6)). Assuming these effects are not present in the right phase we calculated the M function for four configurations. These results suggest that the anomalous dimension is small compared to one. Furthermore we derived the mass for the quarks using the Schwinger function. The result for these masses decreased as we approached the supposed chiral limit. All those results are in agreement with former results [9][10][11][12][6][7][13]. As we argued in section (2.2), this small γ value should not be able to explain the large mass of the top quark. However it is still possible to explain this fact since we have not stated anything about the ETC. It could still be possible to explain the large top mass and the experimental constrains on FCNCs by choosing the right ETC. For this reason the result for γ suggest that the walking dynamics alone will not explain the observed experimental facts.
Apart from the consequences for phenomenology, we were not able to fully investigate the lattice artifacts. One consequence of this fact is the observed finite volume effect for our results. Furthermore we only had four available configurations for our results. An other problem was that the calculation time for the 64×16^3 lattices was too long to get the results from these configurations. This argument shows that again the next step is to first improve the used algorithm. Afterwards we would calculate the results for the 64×16^3 lattices. Furthermore we would change the β and m values. With the new results we could investigate the lattice artifacts further to reduce their influence. On the other hand we want to get closer to chiral limit since the techniquarks should be massless.

References

[1] ATLAS Collaboration, arXiv:1207.7214 [hep-ex]

[2] CMS Collaboration, arXiv:1207.7235 [hep-ex]

[3] ATLAS Collaboration: , http://cdsweb.cern.ch/record/1476765/

[4] J.R. Andersen et. al., arXiv:1104.1255 [hep-ph]

[5] S. P. Martin, arXiv:hep-ph/9709356

[6] L. D. Debbio, B. Lucini, A. Patella, C. Pica, A. Rago, arXiv:1004.3206 [hep-lat]

[7] L. D. Debbio, B. Lucini, A. Patella, C. Pica, A. Rago, arXiv:1004.3197 [hep-lat]

[8] A. Hasenfratz, A. Cheng, G. Petropoulos, D. Schaich, arXiv:1207.7162 [hep-lat]

[9] A. Patella, arXiv:1204.4432 [hep-lat]

[10] J. Giedt, E. Weinberg: arXiv:1201.6262 [hep-lat]

[11] F. Bursa, L. D. Debbio, L. Keegan, C. Pica, T. Pickup, arXiv:0910.4535 [hep-ph]

[12] T. DeGrand, Y. Shamir, B. Svetitsky, arXiv:1102.2843 [hep-lat]

[13] B. Lucini, arXiv:0911.0020 [hep-ph]

[14] A. Bazavov et al. 2009, arXiv:0903.4379 [hep-lat]

[15] C. Gattringer, Phys. Rev. Lett. 97 (2006) 032003; F. Bruckmann, C. Gattringer, C. Hagen, Phys. Lett. B 647 (2007) 56; C. Hagen, F. Bruckmann, E. Bilgici, C. Gattringer, PoS LAT2007 (2007) 289; PoS LAT2008 (2008) 262 [arXiv:0810.0899 [hep-lat]]; E. Bilgici and C. Gattringer, JHEP 0805 (2008) 030

[16] E. Bilgici, F. Bruckmann, C. Gattringer, C. Hagen, Phys. Rev. D 77 (2008) 094007

[17] W. Söldner, PoS LAT2007 (2007) 222

[18] F. Synatschke, A. Wipf, C. Wozar, Phys. Rev. D 75 (2007) 114003; F. Synatschke, A. Wipf, K. Langfeld, Phys. Rev. D 77 (2008) 114018

[19] C. S. Fischer, arXiv:0904.2700 [hep-ph]

[20] J. B. Kogut, M. Stone, H. W. Wyld, S. H.Shenker, J. Shigemitsu, D. K. Sinclair, Nucl. Phys. B 225 (1983) 326

[21] J. B. Kogut, J. Polonyi, H. W. Wyld, D. K. Sinclair, Phys. Rev. Lett. 54 (1985) 1980

[22] J. B. Kogut, Phys. Lett. B 187 (1987) 347

[23] F. Karsch, M. Lütgemeier, Nucl. Phys. Proc. Suppl. 73 (1999) 444

[24] F. Karsch, M. Lütgemeier, Nucl. Phys. B 550 (1999) 449

[25] J. Engels, S. Holtmann, T. Schulze, Nucl. Phys. B 724 (2005) 357 [arXiv:hep-lat/0505008]

[26] F. Sannino, arXiv:0911.0931 [hep-ph]

[27] E. Farhi, L. Susskind, Phys. Rept. 74, 277 (1981)

[28] M. Böhm, A. Denner, H. Joos: Gauge Theories of Strong and Electroweal Interaction, B.G. Teubner 2001

[29] C. T. Hill, E. H. Simmons, Phys. Rept. 381, 235(2003) [arXiv:hep-ph/0203079]

[30] E. Eichten, K. D. Lane, Phys. Lett. B 90, 125 (1980)

[31] E. Witten, Phys. Lett B 117, 324 (1982)

[32] D. D. Dietrich, F. Sannino, K. Tuominen, Phys. Rev. D 72, 055001 (2005) [arXiv:hep-ph/0505059]

[33] R.F. Sobreiro, S.P. Sorella: arXiv:hep-th/0504095

[34] M. E. Peskin, D. V. Schroeder:An Introduction to Quantum Field Theory, Addison-Wesley, 1995

[35] C. S. Fischer: Non-perturbative Propagators, Running Coupling and Dynamical Mass Generation in Ghost-Antighost Symmetric Gauges in QCD, Univ. of Tuebingen. Nov 2002 [arXiv:hep-ph/0304233]

[36] C. Gattringer, C. B. Lang: Quantum Chromodynamics on the Lattice, Springer Verlag 2009

[37] A. Maas: The Standard Model of particle physics, Lecture at the Friedrich Schiller University Jena 2011

[38] I. Montvay,G. Münster: Quantum Fields on a Lattice, Cambridge University Press,1994

[39] L. D. Landau, E. M. Lifschitz, H. Deutsch:Lehrbuch der theoretischen Physik Bd.4, Quantenelektrodynamik, Akademie Verlag 1991

[40] R. Alkofer, W. Detmold, C. Fischer, P. Maris, arXiv:hep-ph/0309077

[41] A. Cucchieri, A. Maas, T. Mendes, arXiv:hep-lat/0605011

[42] W. H. Press, B. P. Flannery, S. A. Teukolsky, W. T. Vetterling :Numerical Recipes in C. The Art of Scientific Computing, 2. Auflage,Cambridge University Press 1992

[43] A. C. Aguilar, J. Papavassiliou 2010, arXiv:1010.5815 [hep-ph]

[44] A. Maas, arXiv:1102.5023 [hep-lat]

[45] L. D. Debbio, B. Lucini, A. Patella, C. Pica, A. Rago, Phys.Rev. D80, 074507 (2009), [arXiv:0907.3896 [hep-lat]]

[46] L. D. Debbio, A. Patella, C. Pica, Phys. Rev. D81, 094503 (2010), [arXiv:0805.2058 [hep-lat]]

[47] T. Kugo, I. Ojima, Prog. Theor. Phys. Suppl. 66 (1979)

[48] K. Osterwalder, R. Schrader, Commun. Math. Phys. 31 (1973) 83-112; Commun. Math. Phys. 42 (1975) 281.

Erklärung

Ich erkläre, dass ich die vorliegende Arbeit selbständig verfasst und keine anderen als die angegebenen Quellen und Hilfsmittel benutzt habe.

.....	.....
Ort, Abgabedatum	Unterschrift des Verfassers

Seitens des Verfassers bestehen keine Einwände, die vorliegende Bachelorarbeit für die öffentliche Nutzung in der Thüringer Universitäts- und Landesbibliothek zur Verfügung zu stellen.

.....	.....
Ort, Abgabedatum	Unterschrift des Verfassers